AD-A121 110 EISCAT ELECTRON DENSITY STUDIES(U) LANCASTER UNIV 1/1
BAILRIGG (ENGLAND) DEPT OF ENVIRONMENTAL SCIENCES
J K HARGREAVES ET AL. 18 JUN 82 AFGL-TR-82-0296
UNCLASSIFIED AFOSR-81-0049 F/G 14/2 NL

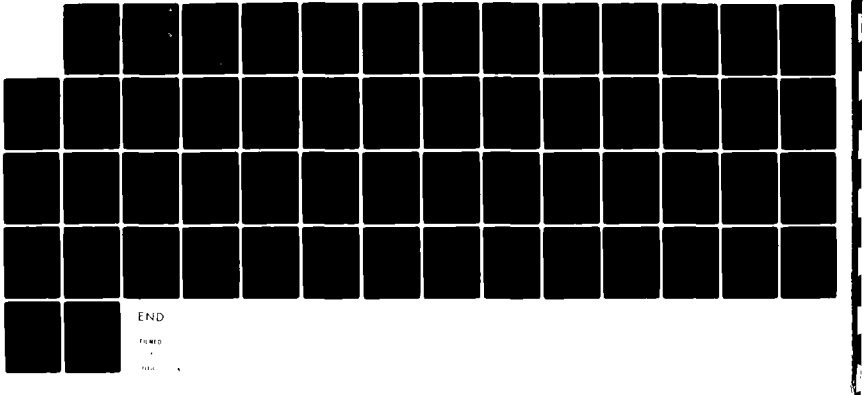

END

FILMED

MICROCOPY RESOLUTION TEST CHART
NATIONAL BUREAU OF STANDARDS-1963-A

MICROCOPY RESOLUTION TEST CHART
NATIONAL BUREAU OF STANDARDS-1963-A

MICROCOPY RESOLUTION TEST CHART
NATIONAL BUREAU OF STANDARDS-1963-A

MICROCOPY RESOLUTION TEST CHART
NATIONAL BUREAU OF STANDARDS-1963-A

AFGL-TR-82-0296

EISCAT ELECTRON DENSITY STUDIES

J.K. Hargreaves and S.C. Kirkwood,
Environmental Sciences Department,
University of Lancaster,
Lancaster. LA1 4YQ
England.

Approved for public release;
Distribution unlimited.

18 June 1982

Final Report 1 May 1981 - 30 April 1982

Prepared for AFGL/PHY, Hanscom AFB, MA 01731,
USA and European Office of Aerospace Research
and Development, London, England.

Qualified requestors may obtain additional copies from the Defense Technical Information Center. All others should apply to the National Technical Information Service.

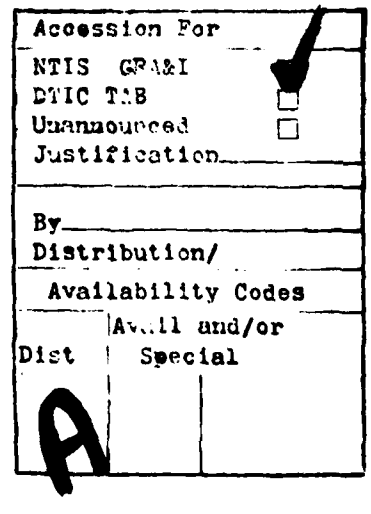

REPORT DOCUMENTATION PAGE		READ INSTRUCTIONS BEFORE COMPLETING FORM
1. Report Number AFGL-TR-82-0296	2. Govt Accession No. AD-A121110	3. Recipient's Catalog Number
4. Title (and Subtitle) EISCAT ELECTRON DENSITY STUDIES		5. Type of Report & Period Covered Final, 1 May 1981-30 April 1982
		6. Performing Org. Report Number
7. Author(s) J.K. Hargreaves and S.C. Kirkwood		8. Contract or Grant Number AFOSR 81-0049
9. Performing Organization Name and Address Environmental Sciences Department University of Lancaster Bailrigg Lancaster LA1 4YQ, England		10. Program Element, Project, Task Area & Work Unit Numbers 61102F 2310G6AC
11. Controlling Office Name and Address Air Force Geophysics Laboratory Hanscom AFB, Massachusetts Monitor/John Klobuchar/PHY		12. Report Date 18 June 1982
		13. Number of Pages 54
14. Monitoring Agency Name and Address EOARD/LNG, Box 14 FPO New York 09510		15. Unclassified

16. & 17. Distribution Statement

Approved for public release; distribution unlimited.

18. Supplementary Notes

19. Key Words

Incoherent Scatter radar; auroral zone; Ionospheric F-region; small-scale plasma irregularities.

20. Abstract

The expected capabilities of the EISCAT incoherent scatter radar facility in measuring small scale-size, small amplitude variations in electron density in the high-latitude F-region ionosphere are discussed. It is shown that it should be possible to observe density irregularities with typical amplitudes down to scale-sizes of 5 km, but for the immediate future system restrictions mean that such small features will be resolvable only in favourable conditions of high ambient electron density and low lateral drifts. Statistical information on time, height and latitudinal variations in irregularity amplitude and occurrence should be obtainable from EISCAT's routine program of measurements. A first analysis of early Common and Special Program data is presented.

FORM 1473

Atch 2

1. Introduction

This report is a study of what we might expect to find out about F-region electron density irregularities using the EISCAT incoherent scatter radar. Some initial observations are included.

A great deal is already known about F-region irregularities from ground-based radio wave observations (scintillation studies) and from in situ measurements made by satellites and rockets. These have provided statistical information on geographic, time of day, seasonal and magnetic activity dependence of irregularity occurrence (summarized in Table 1), on their scale size distribution (a typical example is shown in Fig. 1), and some studies of field alignment and shape have been made (Fremouw and Lansinger, 1981). Measurements using radio waves are however indirect, depending on diffraction of the waves by the irregularity pattern. In general effects may have occurred anywhere along the wave path so the height of scintillation producing irregularities,in particular, is hard to measure. Satellites and rockets measure only along a fixed path so space and time variations cannot be separated. An incoherent scatter radar can measure electron density directly for long periods of time, at several heights simultaneously and at several geographic locations successively and so should be able to provide direct measurements of heights, shapes, sizes, alignments, lifetimes and drifts as well as adding more statistical information on irregularity occurrence. Such information would be invaluable in evalutating the various theories on how irregularities are formed (Fejer and Kelley, 1980).

The major restrictions in using incoherent scatter data for this purpose are the spatial resolution and measurement accuracy. These are determined by the details of the radar facility - beam width and power in particular - and in the case of EISCAT will probably restrict spatial resolution to about 5 km irregularity scale size at 300 km altitude. This is not too severe a

restriction given that the smaller scale scintillation producing irregularities are probably generated by the same mechanism, or a closely related one, as the larger irregularities.

2. The EISCAT Incoherent Scatter Radar

Relevant details of the EISCAT hardware are listed in Table 2. The system transmits according to some predetermined pulse scheme and pointing sequence from Tromso and records the scattered signal at Tromso, Kiruna and Sodankyla. The scattered wave contains information on electron density, temperature and drift and on ion temperature. The remote sites are generally used to determine 3-D drifts, the Tromso receiver being used for the other measurements.

We are primarily interested in electron densities and the accuracy with which these can be measured depends mainly on the range (distance from transmitter to scattering region), the ambient electron density, the transmitted power, the pulse scheme and the integration time for each measurement. Some typical resolutionsare shown in Figure 2, where the pulse scheme is close to those in regular use at EISCAT.

The range resolution is limited by the pulse length and is typically 40-80 km for the pulse schemes currently in use for F-region measurements, the pulse length being chosen to give an adequate power return. This resolution could be greatly improved by pulse coding but this has not yet been implemented at EISCAT.

The lateral resolution (perpendicular to the beam) is limited in the first instance by the beam width : 3 km at 300 km range, 6 km at 600 km range. If a pattern of irregularities drifts through the beam the effective lateral resolution will increase in proportion to the integration time. Since plasma, and consequently irregularity, drifts are expected to be high (Fig. 3) this has a significant effect, as illustrated in Figure 4, for integration times likely

to be used. If the antennae are used to scan (in practice a series of measurements at pre-determined positions) the resolution is further reduced according to the spacing between measurements and the distance the irregularities drift between measurements (Nyquist theorem). Figure 5 shows resolution for various scanning schemes designed to achieve the best possible spatial resolution, given the practical restriction of the system.

Three types of irregularity measurement will be possible:

2-D measurements

If the Tromso antenna points in a fixed direction we will be able to derive statistical information on the time and height variations of irregularity amplitudes and occurrence. Spatial resolution will be limited primarily by integration time, beam-width and drift (Fig. 4).

3-D measurements

If measurements are made at a series of positions (e.g. latitude or longitude scan), for several integration periods at each position we will be able to derive the same information as in the 2-D case and any statistical variation with position in addition. Resolution is the same as in the 2-D case.

4-D measurements

If we use rapid latitude and longitude scanning with closely spaced measurements, one integration period at each point, we should get a complete 4-D picture at least over a small range of latitude and longitude. The resolution now depends also on measurement spacing and antenna move time and, as short integration times will be needed for rapid scanning and smaller scale size irregularities have smaller amplitudes (Fig. 1), will be much more sensitive to the ambient electron density (Fig. 5).

These three types of measurement will be catered for by EISCAT "Common Programs" (2-D, 3-D) and by purpose designed "Special Programs" (4-D).

3. EISCAT Common Programs

These are likely to be similar to the programs outlined below. Common programs are run at times decided at EISCAT HQ, generally during one 24 hour period each week, on a Wednesday. Common programs were run between August and December 1981 with the transmitter at 500 kW and restarted in March 1982 at 2 MW.

CP0

Tromso antenna along field line, remote sites looking at 300 km altitude
pulses 60 μs, 360 μs
short pulse for 100-175 km range, long pulse for 135-750 km
run on 5 occasions, autumn 1982.

CP1

Tromso antenna along field line, remote sites looking at several heights in sequence in the range 95-250 km
pulses 5 x 16 μs, spacing 32 μs, 128 μs, 640 μs
short pulses for E, F1 regions, medium pulses for F, topside,
long pulses for high topside
not yet implemented - simplified form using single 500 μs
pulse run on 7 occasions, autumn 1981.

CP2

Tromso antenna pointing at 3 points in sequence
69.2 N, 19.2 E; 68.4 N, 19.2 E; 68.4 N, 21.1 E at 300 km altitude
pulses 60 μs, 360 μs
cycle time 6 minutes
run on 2 occasions, autumn 1981.

CP3

latitude scan
initially implemented as CP-3 looking at 11 positions covering 5^{o} latitude
pulses 60 μs, 320 μs
cycle time 20 mins

run on 3 occasions, simplified form using 3 positions run on 3 occasions, autumn 1981

Integration times are unpredictable, being chosen to give adequate returns according to conditions prevailing at the time.

4. F-region Irregularity Special Program

4.1. As conceived

A detailed proposal for a rapid scan program was submitted to EISCAT in September 1981 (Appendix I). This proposed

- a scan N by 100 km at 300 km altitude, with measurements every 1 or 2 km, followed by scanning back S, to the starting position.
- a period with the beam stationary and vertical.

Calculation had indicated that we should be able to resolve down to 5 km irregularity scale-size so long as the ambient electron density was fairly high ($> 3 \times 10^{11}$ m^{-3}) and the drift low (Fig. 5a, b). The experiment called for 100 μs pulse length, 1000s pulse repetition rate, 2-3s integration and allowed 0.5 s to move the antenna between positions.

4.2. As implemented

After discussions with EISCAT staff and the UK EISCAT group at the Rutherford and Appleton laboratories the scheme was slightly modified. System constraints meant that a 4s integration was the shortest achievable, 4s had to be allowed to move the antennae as their response is delayed and a 250 μs pulse had to be used since the system power was then only 500 kW and only 2 out of the proposed 8 frequencies were available, thus restricting the effective pulse repetition rate. In order to avoid a degradation of lateral resolution at the extremes of the scan and to avoid going through zenith, the scan sequence was changed to a cross pattern centered on the Tromso field line. To allow rapid repetition of scans, the sequence was changed to:

- a period of measurements with the Tromso beam stationary and looking up the field line (azimuth 179.8, elevation 76.51)

- an elevation scan N by 100 km at 300 km altitude, with measurements every 2 km, starting 50 km S of the field line (azimuth 179.8, elevation 67.07) and ending 50 km N of the field line (azimuth 179.8, elevation 86.07), followed by a scan back S, back N and back S.
- a second period of measurements with the Tromso beam stationary and looking up the field line.
- an azimuth scan W by 100 km at 300 km altitude, with measurements every 2 km, starting 50 km E of the field line (azimuth 170.3, elevation 76.51) and ending 50 km W of the field line (azimuth 189.30, elevation 76.51) followed by a scan back E, back W, and back E.

The predicted resolution with this scheme is shown in Figure 5d (where only single frequency operation has been assumed, as problems have occured using 2 frequencies), with 5c representing what should be achieved with the same scheme once power is increased to 2MW and 2 frequency operation is logged successfully.

As can be seen from Figure 5, the greatest restriction to the resolution is the drift and since this is likely to be low during the day or near midnight (Fig. 3) but irregularities are more likely to occur over Tromso at night (Table 1), it was proposed that the experiment be run, at least initially, near midnight. We would hope to see, at best, individual irregularities, displaced on consecutive scans so that their variation with height, scale-sizes and drift could be seen. If drift were too high, we should get an irregularity spectrum displaced in frequency for scans in opposite directions and for the stationary measurements. This could again lead to measurements of drift, scale-size distribution and height variation. Tristatic measurements of plasma drift at 300 km would be included for comparison.

This program was implemented at EISCAT by T. Van Eyken (UK EISCAT group, RAL) and two hours of reasonable data were collected, as described below.

However, because of the low system power and consequent requirement for a high ambient electron density the program was run in late afternoon and appears not to have detected any significant irregularity! (The local K index was 2, and irregularities are present about 10% of the time in such conditions; Clark and Raitt, 1976). It will be run again after revision of the radar controller programs to improve the data logging, as soon as possible. It is also planned, once irregularities have been measured successfully overhead at Tromso, to look at the sub-auroral zone (approx. overhead Kiruna) and the polar zone > 70^{0} N, but pulse coding will probably be required before reasonable resolution can be attained with the low elevations required.

5. Data Analysis and Initial Results

5.1. Methods of analysis

The raw data of the EISCAT system are autocorrelation functions which are the Fourier transform of the signal power spectrum, after scattering by ionospheric electrons, convolved with system gating functions and added to noise. Extracting useful data from these"acfs"- electron densities, temperatures and drift velocities and ion temperatures - requires sophisticated analysis,and software packages to do the reduction are being developed by EISCAT staff and by the U.K. EISCAT group at RAL and reduced data should be available routinely, but as this will probably be at a lower time resolution than the original measurements we will need to access the raw data and process it specially. So far, only electron densities (uncorrected for temperature) can be derived routinely and directly. Even these are not very accurate in absolute terms, the system being uncalibrated so that ionosonde measurements have to be used for scaling.

Data can be accessed by requesting copies of tapes from EISCAT HQ and reading from these tapes using utilities largely provided by RAL, further analysis currently being done using programs written at Lancaster University (Table 3). Uncorrected electron densities can be derived simply by subtracting background [illegible] from the scattered signal-plus-noise power returned from a

particular range interval (the zero-lag acf in the corresponding time interval), correcting for the range (multiplication by range squared) and multiplying by a suitable scale factor chosen to give an F-peak electron density corresponding to that measured by an ionosonde.

The receiver noise is determined by measuring the power in the receiver after all scattered signal is presumed to have returned (in practice the return from > 1500 km is assumed to be negligible).

Electron densities derived in this way are illustrated in Figures 6 and 10, for the rapid scanning Special Program run on 17 December 1981 and for a Common Program run on 20 August 1981, respectively. In order to examine variations in electron density, we further process the data by taking the percentage variation about a best fit straight line for the time series of electron densities at each range. Plots showing irregularities derived in this way are illustrated in Figures 7 and 12. In both figures the shortest period variations have been filtered out as they are not likely to include useful information and may mask the longer period variations. The longest period variations have also been filtered out in Figure 12 as they are considered not to be "irregularities" (they comprise daily variations, gravity waves etc.) Irregularity power spectra for the two sets of data are given in Figures 9 and 13.

5.2 Significance of results

Next we must consider what these apparent variations represent. The measured electron density will always appear irregular, to a certain extent, because of the statistical uncertainty in each measurement. The predicted statistical uncertainties (the white noise in the spectra) for the ambient conditions and the appropriate pulse schemes are shown in Figures 6 and 11. The corresponding power levels are marked on the spectra and the consequent maximum irregularity sizes (4 x the uncertainty, peak-to-peak) are shown as

bars opposite the ends of the irregularity plots for corresponding ranges.

In the case of the 17 December data it is clear that most of the apparent variation in electron density is close to the expected noise level. On the 20 August, however, the predicted noise levels are lower and there seem to be significant variations with amplitudes well above the noise level, particularly at lower altitudes (Fig. 12). The irregularities are apparently field-aligned, occurring over several ranges simultaneously. However, this is also what we would expect to see if the transmitted power fluctuated. This data was collected soon after EISCAT started working for the first time and there were several obvious power drop-outs, which were deleted from the data before processing. Since there is as yet no monitor of transmitted power it is impossible to tell whether any individual irregularity is real or simply a power fluctuation. We shall simply note that there may be real irregularities present, decreasing in amplitude with decreasing period (i.e. scale size if we assume some drift.)

The 17 December 1981 data requires more consideration. Although the variations in Figure 7 are close to the predicted noise level they do not appear random but occur simultaneously for all ranges, particularly towards the end of the second scanning sequence. This is in fact a result of the analysis - the noise value subtracted at each point is an instantaneous measurement and fluctuates considerably from one measurement to the next. When the signal to signal-plus-noise ratio is close to 1, as here, a peak in the noise, for example, results in an apparent dip in the electron density at all ranges. Since we are looking for true field alignment, this effect is distracting so the data has been reprocessed using a uniform noise measurement for all the data (Fig. 8). A disadvantage to this technique is that it makes no allowance for genuine variations in background noise. This is illustrated by the peak apparent on repeated scans and at all ranges in the second frame of Figure 8. Its negligible rate of drift makes it likely that this is a radio-star

and in fact the position and time are appropriate for Cassiopeia A. Evidently some more sophisticated method of deriving a smoothed estimate of background noise variations will have to be developed before any small features can be identified as true electron density variations.

Conclusions

The EISCAT system will evidently be capable of making meaningful measurements of the larger F-region electron density irregularities (> 5 km scale size). The noise levels are close to those expected, and fairly rapid scanning and data logging have been achieved. Until recently, due to administrative problems, very little data was generally accessible. That has now changed, so that several complete 24 hour periods of recording of common program data are now available and should provide good statistical information on irregularity occurrence. Use of the rapid scanning program, in suitable conditions, i.e. reasonably high magnetic activity, low drifts, should give direct measurements of irregularity shapes and sizes, now that the system is working at full power.

Acknowledgements

This research has been sponsored in part by European Office of Aerospace Research and Development. The staff of the UK EISCAT group at the Rutherford and Appleton Laboratory, particularly Dr. T. Van Eyken have given advice and support. C.M. Hall and B.K. Madahar gave assistance with software development. Data was received from the EISCAT Scientific Association, an association of Government funded Research Agencies in six countries (Finland, France, Germany, United Kingdom, Norway, Sweden) responsible for the installation and operation of an incoherent scatter facility in Northern Scandinavia.

References

Phelps, A.D.R., Sagalyn, R.C. Plasma density irregularities in the high latitude topside ionosphere. J. Geophys. Res. 81, 515-523, 1976.

Frihagen, J. Irregularities in the electron density of the polar ionosphere. In: The polar ionosphere and magnetospheric processes, G. Skovli, ed. : pp. 271-284. New York: Gordon and Breach 1970.

Sandford, B.P. Optical emission over the polar cap. In: The polar ionosphere and magnetospheric processes, G. Skovli, ed. : pp. 299-321. New York: Gordon and Breach 1970.

Fejer, B.G., Kelley, M.C. Ionospheric irregularities. Rev. Geophys. Space Phys. 18, 401-454, 1980.

Fremouw, E.J. and Lansinger, J.M. Dominant configurations of scintillation producing irregularities in the auroral zone. J. Geophys. Res. 86, 10087-10094, 1981.

Clark, D.H. Raitt, W.J. Characteristics of the high latitude ionospheric irregularity boundary as monitored by the total ion current probe on Esro-4. Planet. Space Sci. 23, 1643-1647, 1975.

Clark, D.H., Raitt, W.J. The Global morphology of irregularities in the topside ionosphere as measured by the total ion current probe on Esro-4. Planet. Space Sci. 24, 873-881, 1976.

Sojka, J.J., Raitt, W.J., Schunk, R.W. High latitude plasma convection: predictions for EISCAT and Sondre Stromfjord. Geophys. Res. Lett. 6, 877-880, 1979.

Fig. 1. Power spectra of electron density variations recorded by ISIS-1 during a pass over the southern polar region at altitudes 590-1600 km. Passes over the N pole show spectra of similar shape (after Phelps and Sagalyn, 1976).

Fig. 2. Representative model electron density profiles and corresponding predicted uncertainties in electron density determination using EISCAT. Assumes integration times of 60s and 8s which are among those used in the EISCAT Common Programs, pulse length 320 μs, pulse repetition rate 100 Hz, transmitter power 2 MW, noise 30 K. Calculations by EISCAT planning program (author P. Williams).

Fig. 3. Predicted distribution of horizontal F-region plasma drifts for different magnetospheric field models (after Sojka et al., 1979).

Fig. 4. Irregularity scale size resolution for measurements with EISCAT beam in a fixed direction, as a function of irregularity drift speed and measurement integration time T. b is the beam width at 300 km range. It is assumed that the accuracy of relative electron density determination is arbitrarily high.

Fig. 5. Irregularity scale-size resolution using EISCAT, as a function of irregularity drift speed, for a rapid latitude or longitude scan. Solid lines represent the restriction due to effective measurement spacing which is the true spacing plus the distance drifted between consecutive measurements; + is for scanning in the same sense as the drift, - against the drift. Dashed lines are restrictions due to the accuracy of relative electron density determination, smaller scale-size irregularities having smaller amplitudes (assuming $\Delta N/N$ (at 50 km) = 10%), for 4 different ambient electron densities : 1.3×10^{12}, 2.1×10^{12}, 3.3×10^{11}, 4.1×10^{11}. Long-dashed

lines are the limits for individual irregularities, short-dashed lines are for continuous wave-like irregularities to be resolvable in a spectrum. The dotted line b is the beam width. All figures relate to 300 km altitude/range.

a) assumes peak power 2 MW, pulse length 100 μs, pulse repetition rate 1000 Hz, noise 30 K, 2s integration, 2s antenna move time. This represents the best possible resolution likely to be achievable at high drift speeds.

b) as a) but 4s integration to give better results at low drift speeds.

c) as b) but 4s antenna move time, pulse length 250 μs, pulse repetition rate 250 Hz, noise 300 k. Likely to be the best achievable in the immediate future (Spring 1982).

d) as c) but pulse repetition rate 125 μs, peak power 500 kW. Represents likely resolution of Special Program run in December 1981

Fig. 6. 17 December 1981 : electron density profiles derived from EISCAT measurements, with ionosonde calibration at 1500, 1600 and 1700 UT and associated predicted accuracy of relative electron density determinations (integration time 4s, pulse length 250 μs, pulse repetition rate 125 Hz, power 500 kW, noise 300 k).

Fig. 7. 17 December 1981 : variations in apparent electron density for two sequences of 4 latitude scans between the elevations shown, at an azimuth of 179.8 deg. There are 4 ranges represented : 262.5,300.0, 337.5,375.0 km. Times marked are for the middle of each scan, each scan taking 400s. The small bars opposite the plots for 300.0 and 375.0 km ranges represent the maximum predicted size of noise variations. Data reduced using instantaneous measurements of noise and filtered to reduce short wavelengths.

Fig. 8. As Fig. 7. but data reduced using uniform noise level (see text).

Fig. 9. 17 December 1981 : irregularity power spectra for 1500-1600 and 1600-1700, UT. Dashed line is the predicted statistical "noise" level.

Fig. 10. 20 August 1981 : contours of electron density determined from EISCAT measurements, calibrated by ionosonde. Pulse scheme as for CP-1 (see text): beam along field-line, 500 μs pulse length, pulse repetition rate 100 Hz, system power 500 kW, integration time 60s.

Fig. 11. 20 August 1981 : representative predictions of accuracy in relative electron density determination corresponding to 1800 hours in Fig. 10.

Fig. 12. 20 August 1981 : apparent irregularities in electron density at times and ranges shown. Data filtered with 8-32 min passband. Bars at right hand side show predicted maximum size of noise "irregularities".

Fig. 13. 20 August 1981 : irregularity spectra for 1730-2130, UT. Dashed line represents predicted level of statistical "noise".

Table 1 High latitude irregularity characteristics. Note that upper limit to altitude range is upper limit of observations, not necessarily limit of irregularities. Except where marked, information is from Clark and Raitt, 1975 and 1976[6,7].

Zone	Location	Average Intensity $(\Delta N/N)_{RMS}$	Occurrence	Possible Production Mechanism
polar zone	$>72^{o}$-84^{o}, midnight $>65^{o}$-82^{o}, noon	moderate - strong (6-10%)	all times, all altitudes (400^{2}-3500^{1}km)	poleward motion of irregularities generated in auroral zone
auroral zone	[3]varies with magnetic activity 64^{o}-74^{o}N, midnight 72^{o}-74^{o}N, noon for Kp $\sim$ 3	strong (8-10%)	all times, all altitudes (350^{2}-3500^{1} km) Increasing intensity and equatorward movement of boundary with increasing Kp	1) particle precipitation 2) electrostatic turbulence 3) [4]plasma instabilities
sub auroral zone	between 50^{o}-60^{o} and 64^{o}N, midnight	moderate (4-6%)	only at night, all altitudes (300^{2}-3500^{1} km) Equatorward movement of boundary with increasing Kp.	1) [4]equatorial motion from creation in auroral zone 2) magnetospheric heat conduction 3) heat transfer from ring current 4) heating effect of conjugate photo electrons in winter

[1]Phelps, A.D.R., Sagalyn, R.C., 1976
[2]Frihagen, J., 1970.
[3]Sandford, B.P. 1970
[4]Fejer, B.G., Kelley, M.C., 1980.

Table 2. Details of EISCAT System (VHF)

Location	Tromso (T_x, R_x)	66.6^{o}N, 104.9^{o}E (corrected geomagnetic)
	Kiruna (R_x)	64.9^{o}N, 104.2^{o}E
	Sodankyla (R_x)	63.9^{o}N, 108.5^{o}E
Antennae	Diameter 32 m	
	Half-power beam width 0.6^{o}	
	Steerability: elevation 10^{o} - 90^{o}; azimuth $\pm 270^{o}$	
	Maximum slewing rate 80^{o}/minute	
Transmitter	*Frequency* 933.5 ± 2.5	
	(choice of 8 frequencies in 0.5 MHz steps - 2 only available, Spring 1982)	
	Peak power output 2 MW (0.5 MW only up to December 1981)	
	Average power 250 kW	
	Pulse repetition rate 0 - 1000 Hz	
	Pulse length 10 μsec - 10 msec, variable	

Table 3. Data processing software

Program/Utility name	Major routines called	Description	Length (lines)	Language	Author
TAPEIDX		Prints index of files on EISCAT raw data tape.	150	FORTRAN H MVT JCL	C.M. Hall
TAPETXT		Prints text files from EISCAT raw data tapes.	200	FORTRAN H MVT JCL	RAL EISCAT group
TAPEDAT		Reads raw data files from EISCAT tapes and stores to disk.	450	FORTRAN H MVT JCL	RAL EISCAT group
	RNORD	Routine to convert from integer format to NORD real	20	IBM Assembler	RAL Systems group
ZLAGEX		Extracts zero-lag acf's and system parameter information from disk files output by TAPEDAT. Lists to line printer or stores on disk.	130	FORTRAN 77 CMS JCL	S. Kirkwood
	RNORD	Routine to convert from integer format to NORD real.	50	FORTRAN 77	S. Kirkwood
ZLAGPR		Reduces zero-lag acf's to uncorrected electron densities.	60	FORTRAN 77	S. Kirkwood
DENAN1		Processes electron densities to give % variations about mean. Filters, computes spectra, outputs line printer plots and files of reduced data.	1000	FORTRAN 77	S. Kirkwood
	LPGR1	Draws line printer plots of multiple time series.	250	FORTRAN 77	C.M. Hall
	BPFIL	Two-pass phaseless time-domain bandpass filter with variable window length and cut-offs.	130	FORTRAN 77	Anon.
	COOL	Fast fourier transform.	80	FORTRAN 77	Anon

Table 3. (continued)

Program/Utility Name	Major routines called	Description	Length (lines)	Language	Author
GPLOT2		Plots electron densities and % variations as a function of time and range. Output can be on a VDU or via FR80 film camera to 16 mm or 35 mm film (colour or B/W), microfiche (B/W) or paper (B/W).	1200	FORTRAN G SMOG	S. Kirkwood
	CNTR2B	General purpose contouring routine for irregularly spaced grid.	-	-	RAL Systems group
	CC2	General purpose pixel type colour 'contouring' routine with 12 colour levels.	300	FORTRAN G	C.M. Hall
	DNPLOT	Routine to draw multiple time series, with automatic scaling.	200	FORTRAN G	B.K. Madahar
PPLOT		Plots power spectra output by *DENAN1*.	300	FORTRAN G	S. Kirkwood
STACK1		Stacks irregularity/time series for several ranges. Computes auto and cross-correlation between time series. Plots and files results.	550	FORTRAN G	B.K. Madahar
EISCAT		EISCAT planning program - predicts S/S+N ratios and integration periods required for 5% accuracy for an input pulse scheme and pointing direction.	900	FORTRAN G	P. Williams (EISCAT Staff)

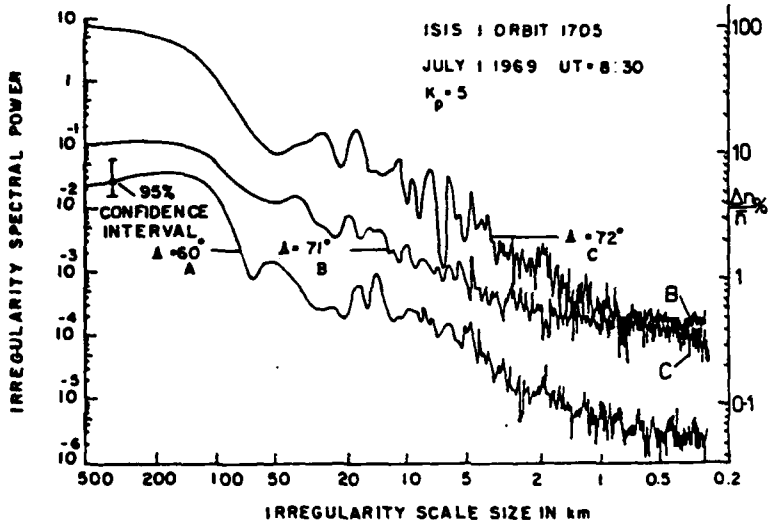
ISIS I ORBIT 1705
JULY 1 1969 UT = 8:30
K_p = 5
95% CONFIDENCE INTERVAL
Δ = 60° A
Δ = 71° B
Δ = 72° C
IRREGULARITY SPECTRAL POWER
IRREGULARITY SCALE SIZE IN km
$\frac{\Delta n}{n}$ %

Figure 1

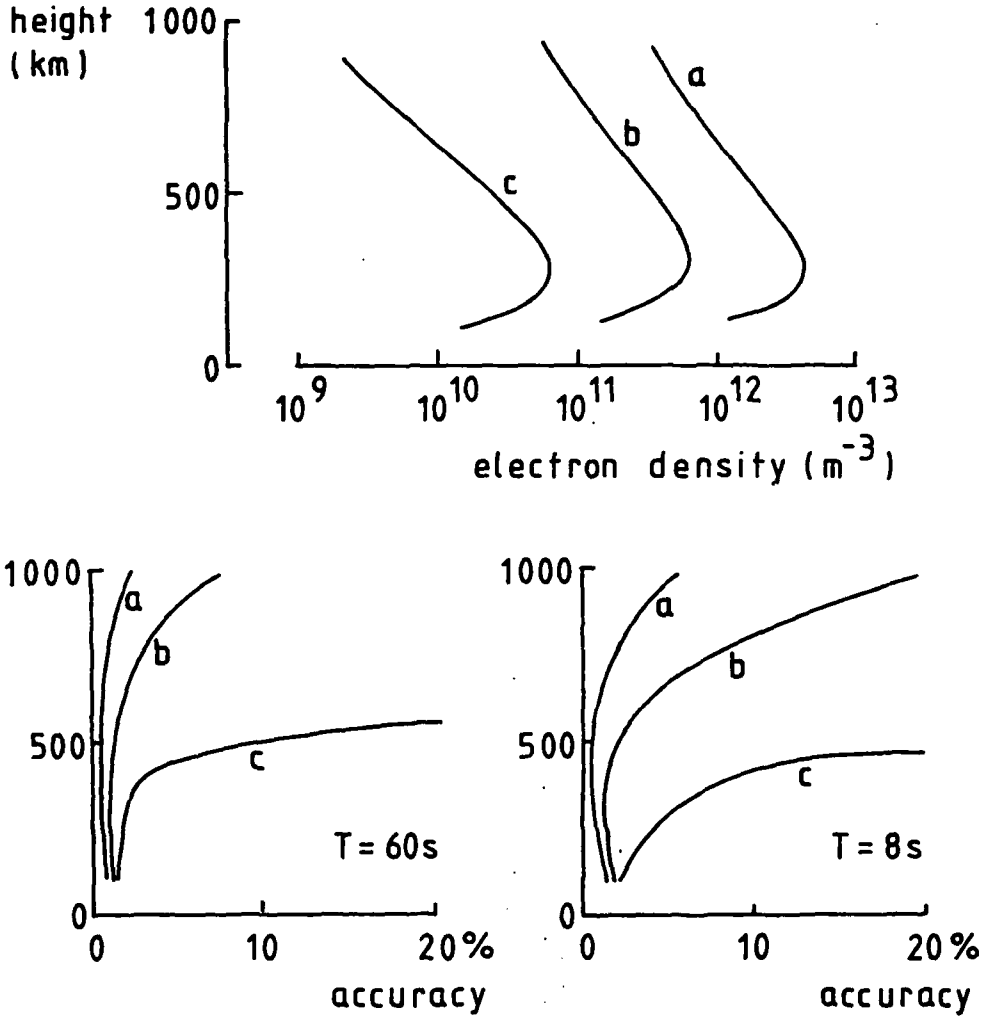
height (km)
1000
500
0
a
b
c
10^9
10^{10}
10^{11}
10^{12}
10^{13}
electron density (m^{-3})
1000
500
0
a
b
c
T = 60s
0
10
20%
accuracy
1000
500
0
a
b
c
T = 8s
0
10
20%
accuracy

Figure 2

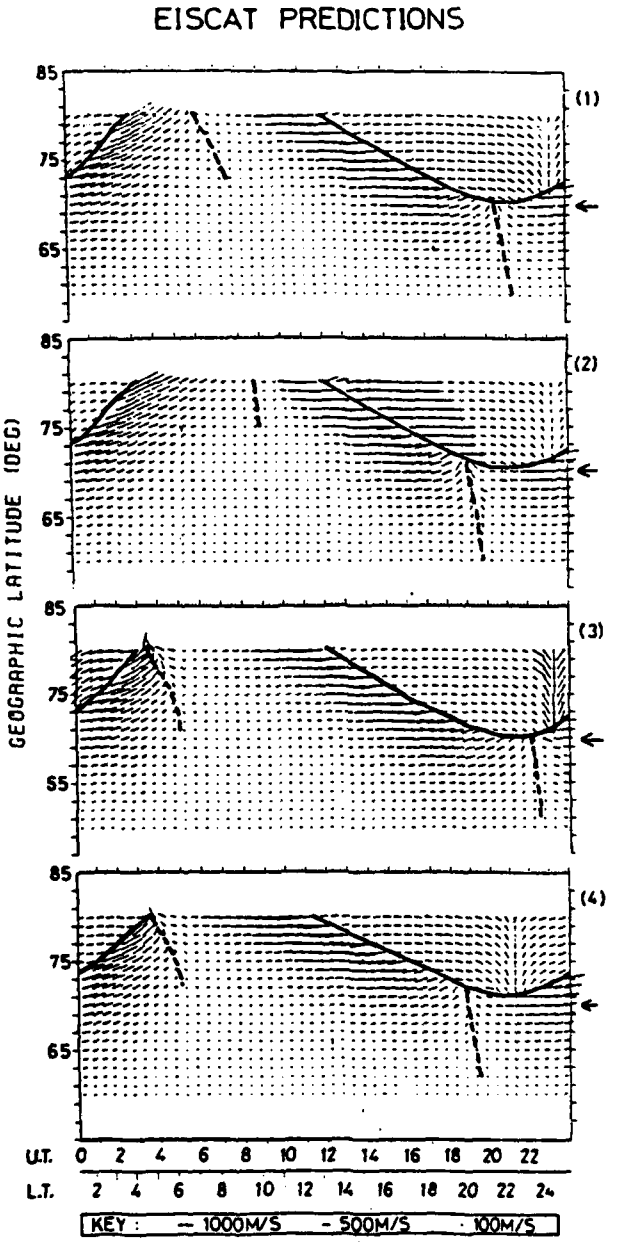
EISCAT PREDICTIONS
85
75
65
(1)
(2)
(3)
(4)
GEOGRAPHIC LATITUDE (DEG)
U.T. 0 2 4 6 8 10 12 14 16 18 20 22
L.T. 2 4 6 8 10 12 14 16 18 20 22 24
KEY : — 1000M/S - 500M/S · 100M/S

Figure 3

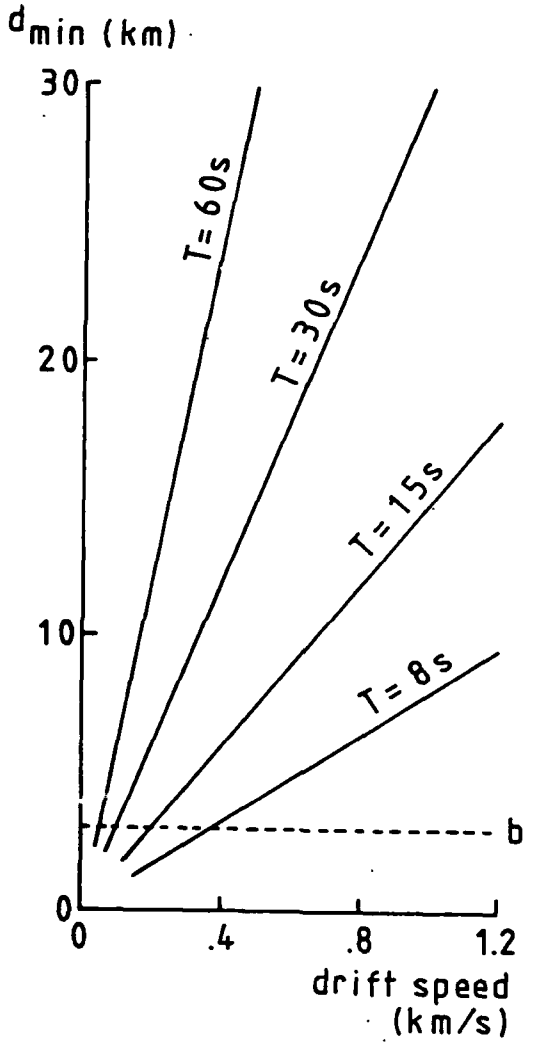

Figure 4

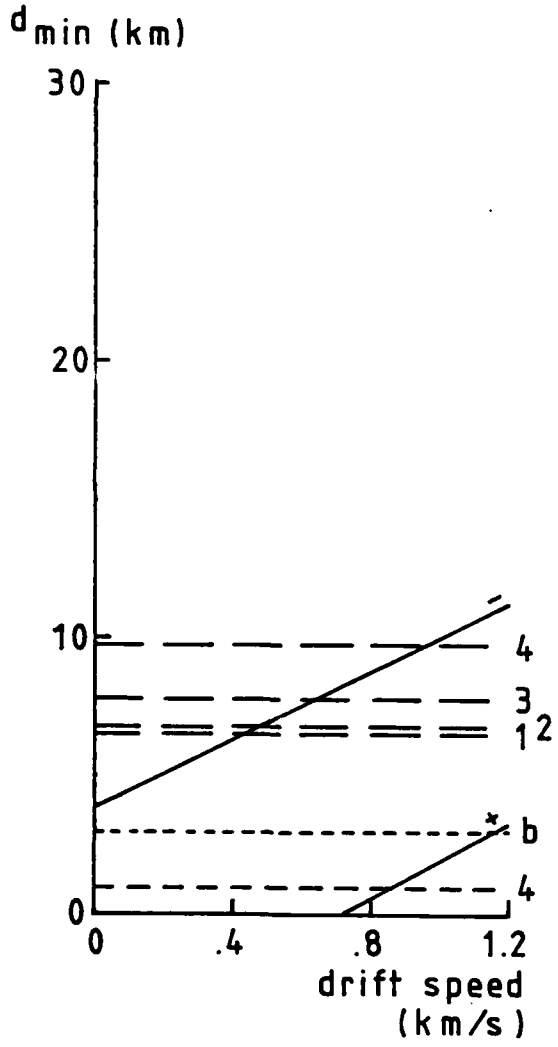

Figure 5(a)

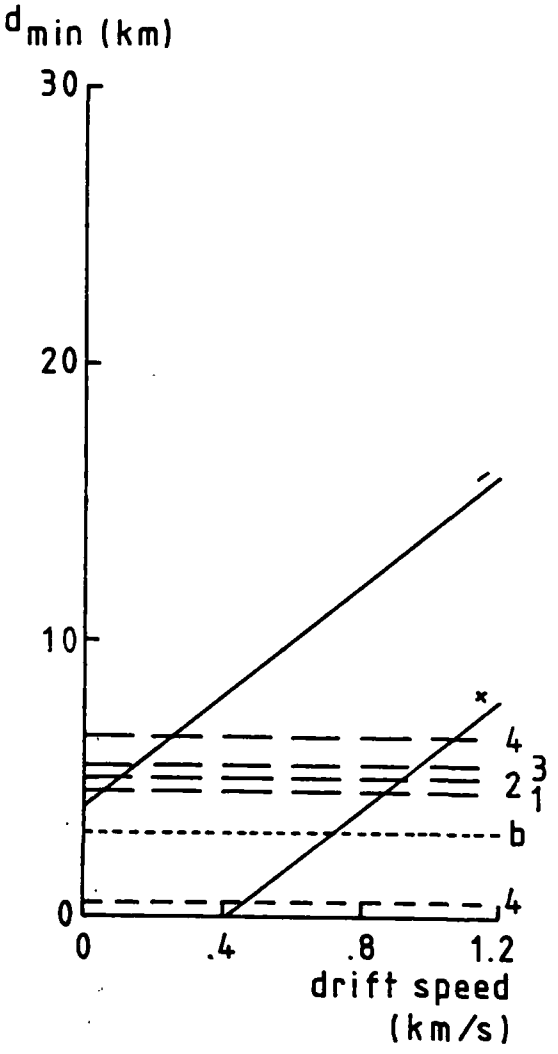

Figure 5(b)

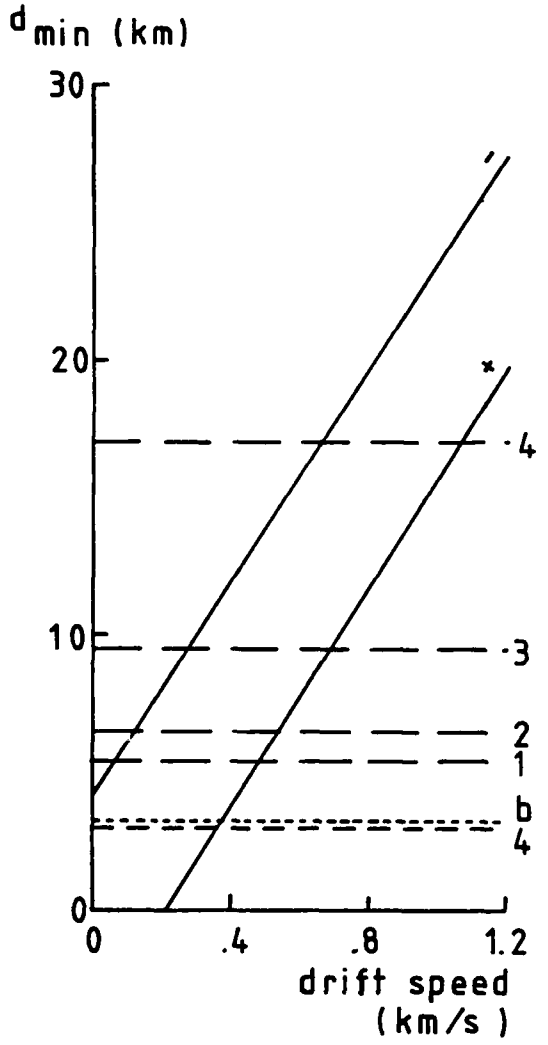

Figure 5(c)

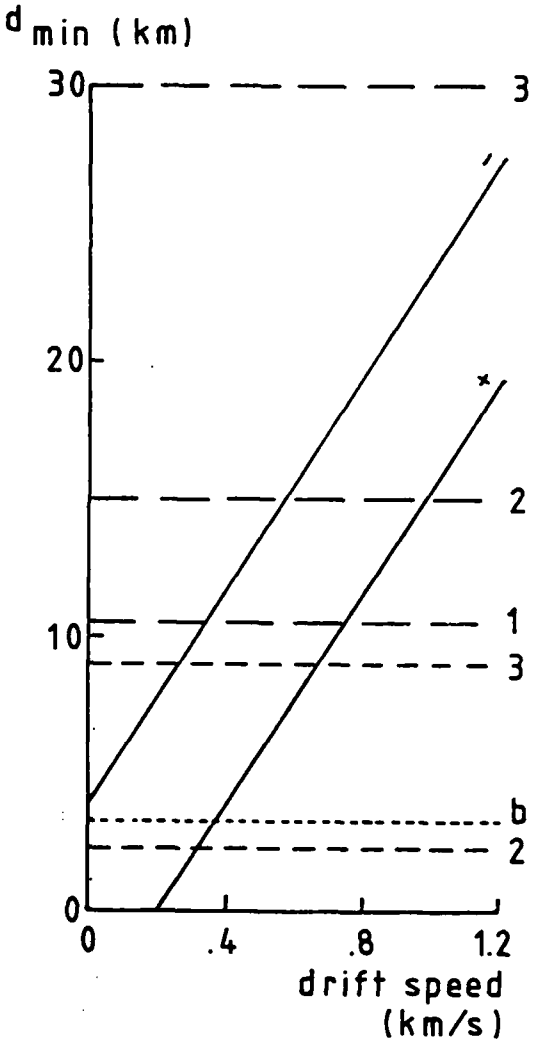

Figure 5(d)

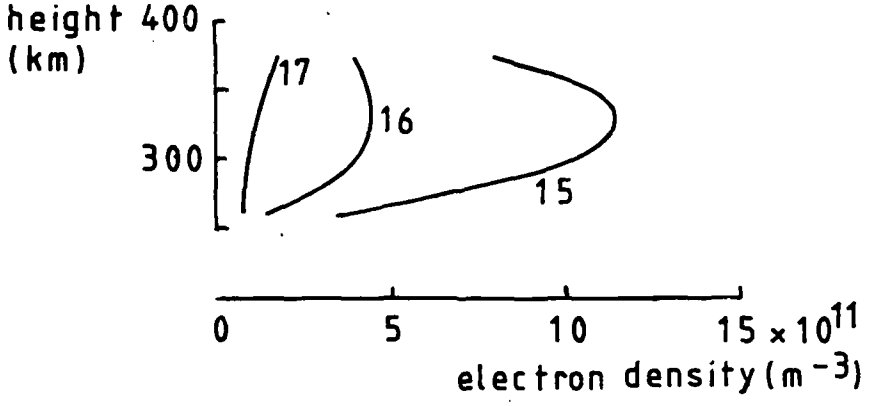
height
(km)
400
300
17
16
15
0
5
10
15 x 10^11
electron density (m^-3)

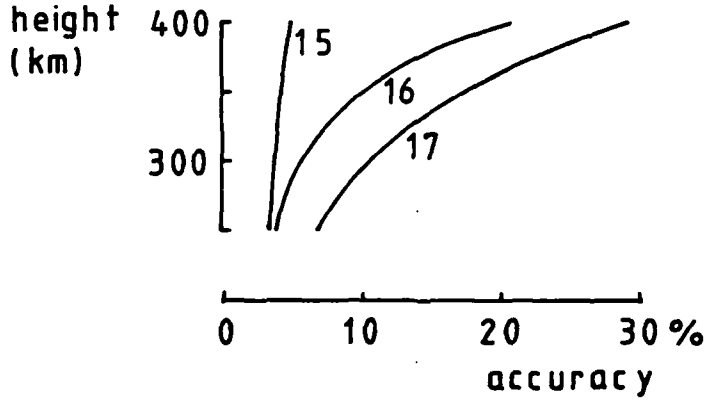
height
(km)
400
300
15
16
17
0
10
20
30 %
accuracy

Figure 6

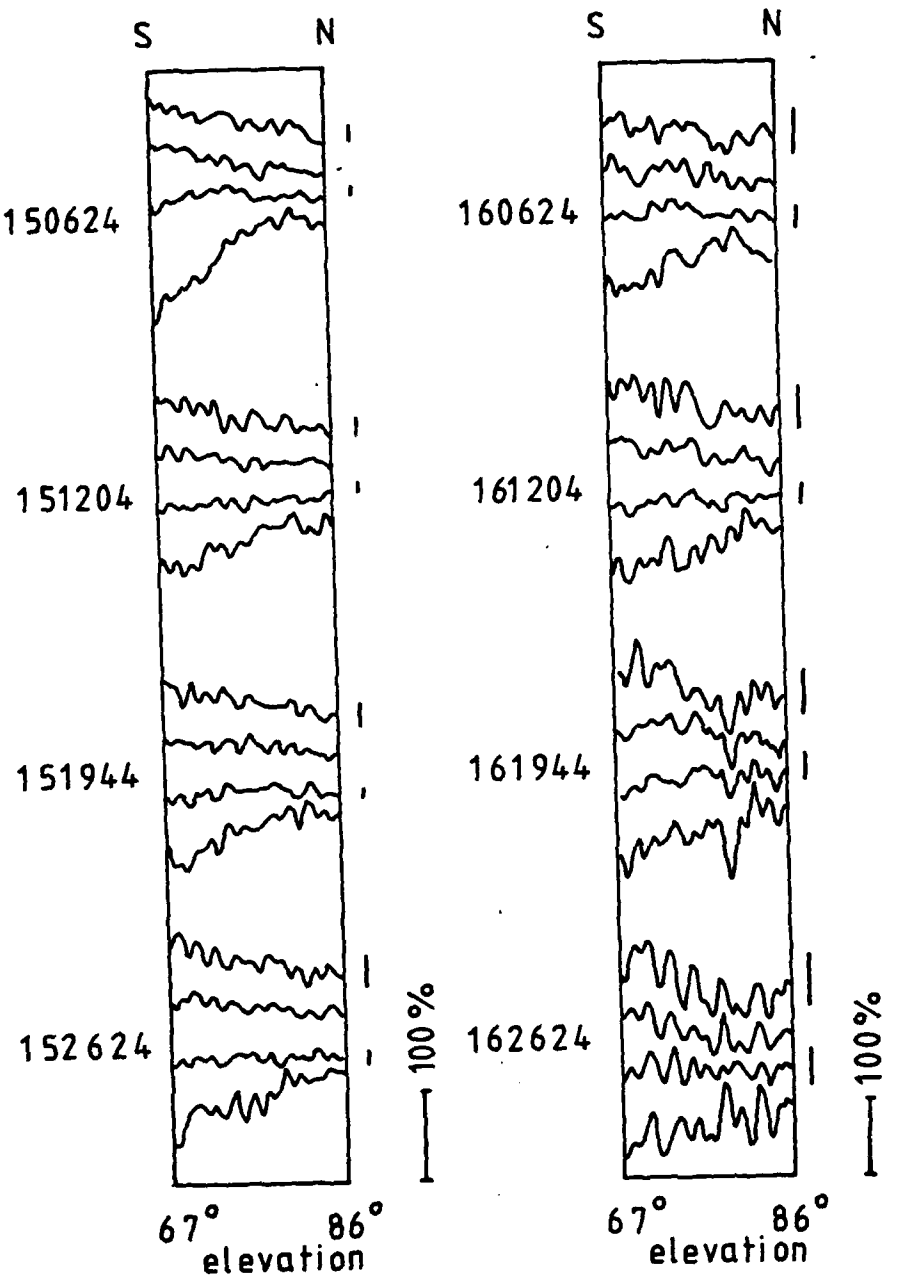
S
N
150624
151204
151944
152624
100%
67°
86°
elevation
S
N
160624
161204
161944
162624
100%
67°
86°
elevation

Figure 7

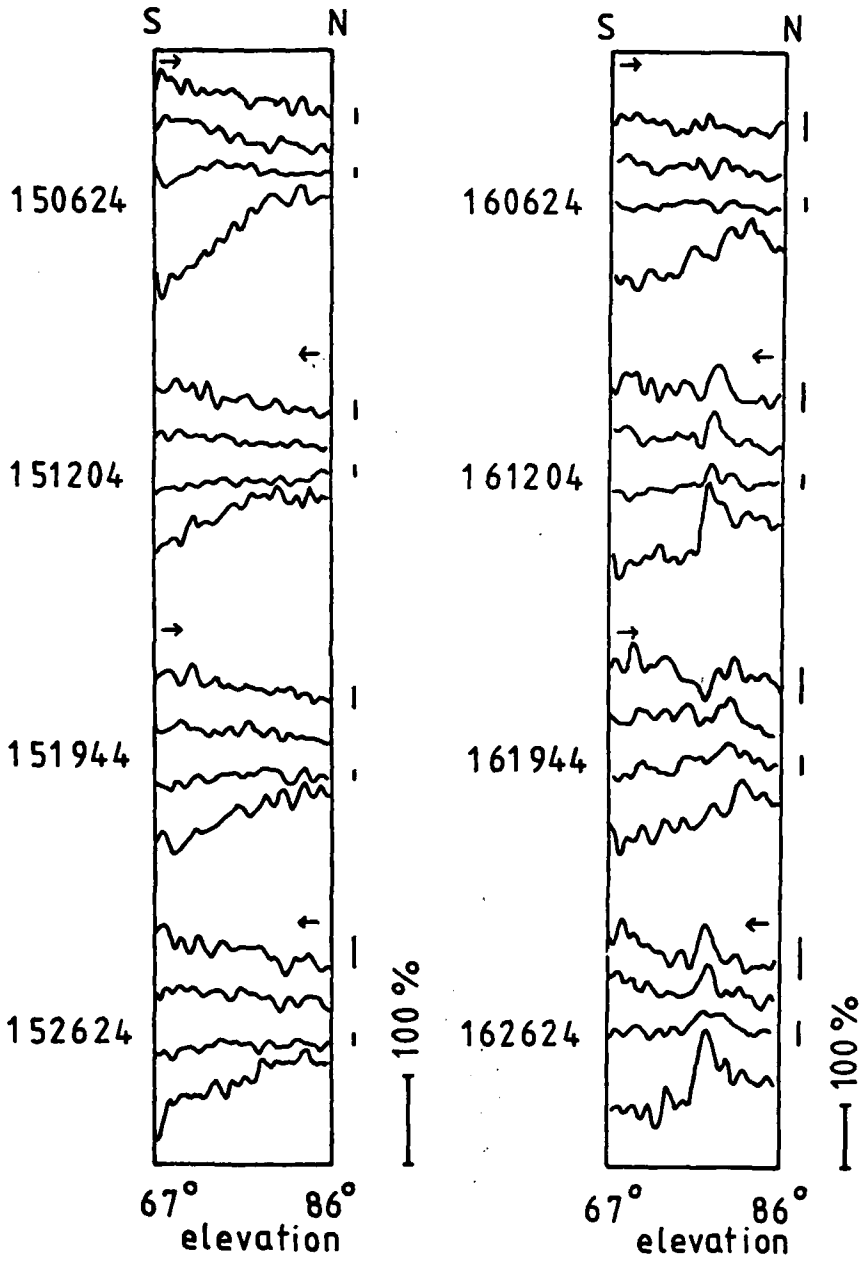
S
N
150624
151204
151944
152624
100 %
67°
86°
elevation
S
N
160624
161204
161944
162624
100 %
67°
86°
elevation

Figure 8

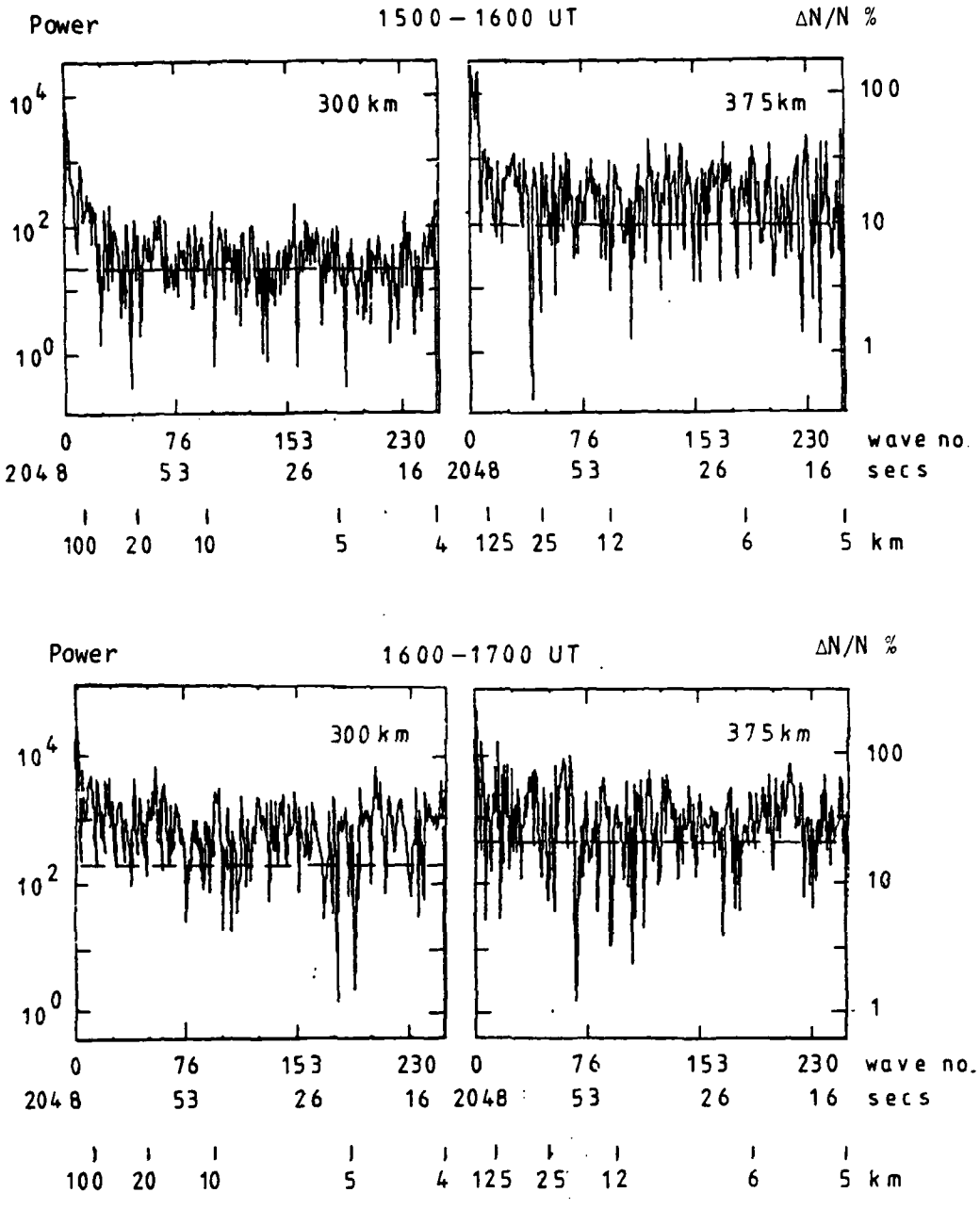
Power
1500 – 1600 UT
ΔN/N %
300 km
375 km
10^4
10^2
10^0
100
10
1
0 76 153 230 0 76 153 230 wave no.
2048 53 26 16 2048 53 26 16 secs
100 20 10 5 4 125 25 12 6 5 km
Power
1600 – 1700 UT
ΔN/N %
300 km
375 km
10^4
10^2
10^0
100
10
1
0 76 153 230 0 76 153 230 wave no.
2048 53 26 16 2048 53 26 16 secs
100 20 10 5 4 125 25 12 6 5 km

Figure 9

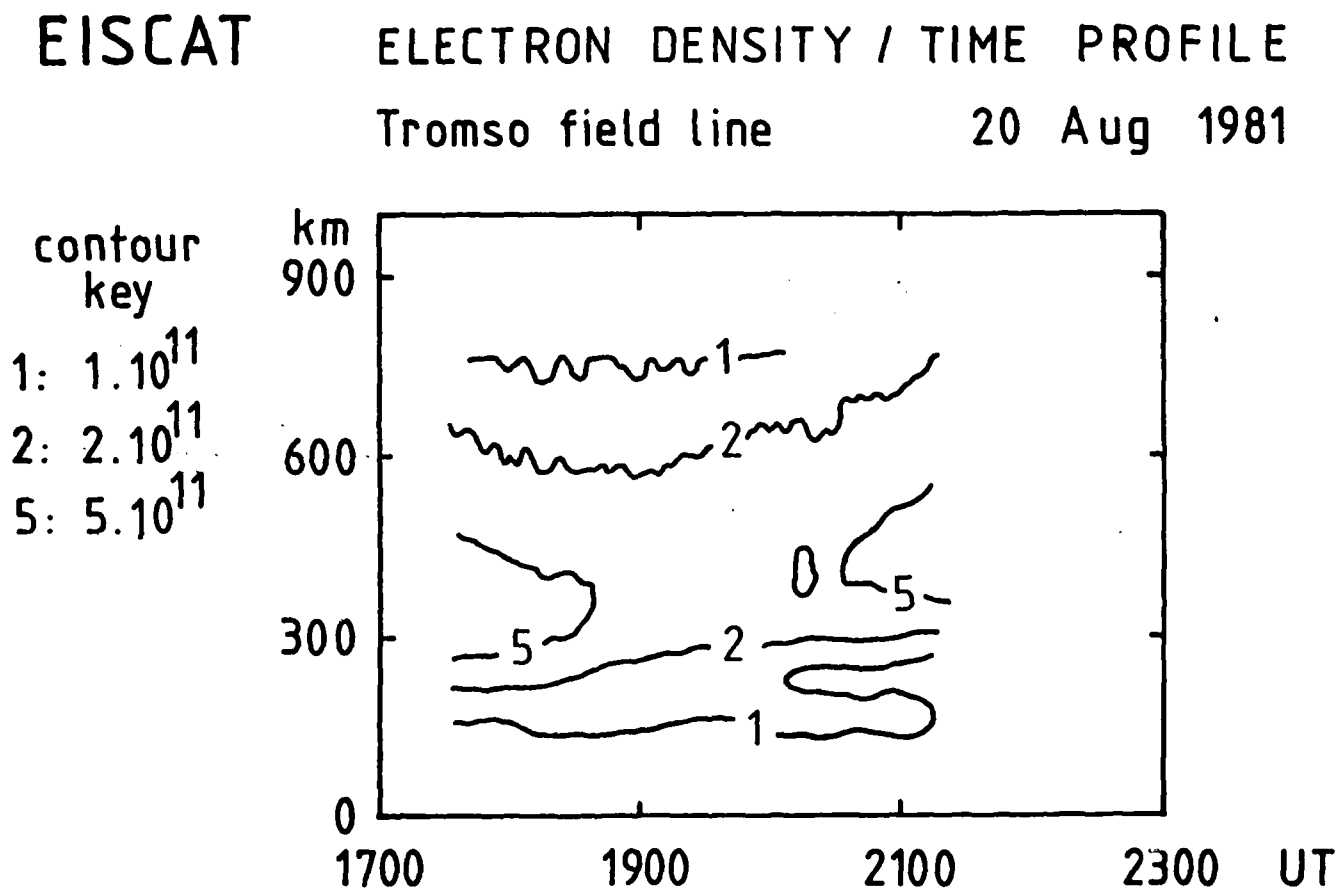
EISCAT
ELECTRON DENSITY / TIME PROFILE
Tromso field line
20 Aug 1981
contour key
1: 1.10^11
2: 2.10^11
5: 5.10^11
km
900
600
300
0
1700
1900
2100
2300
UT
1
2
5
0
5
2
1

Figure 10

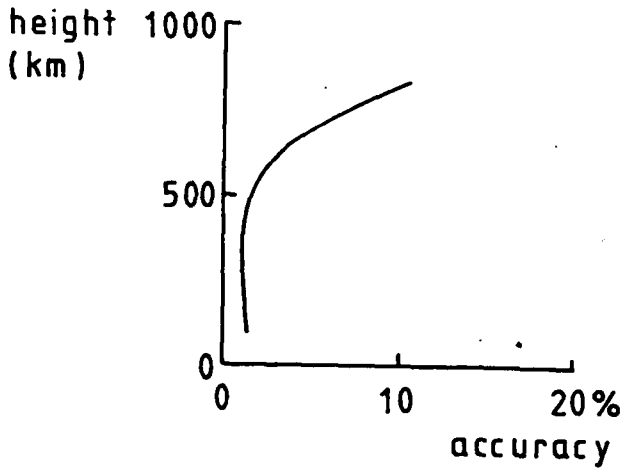

Figure 11

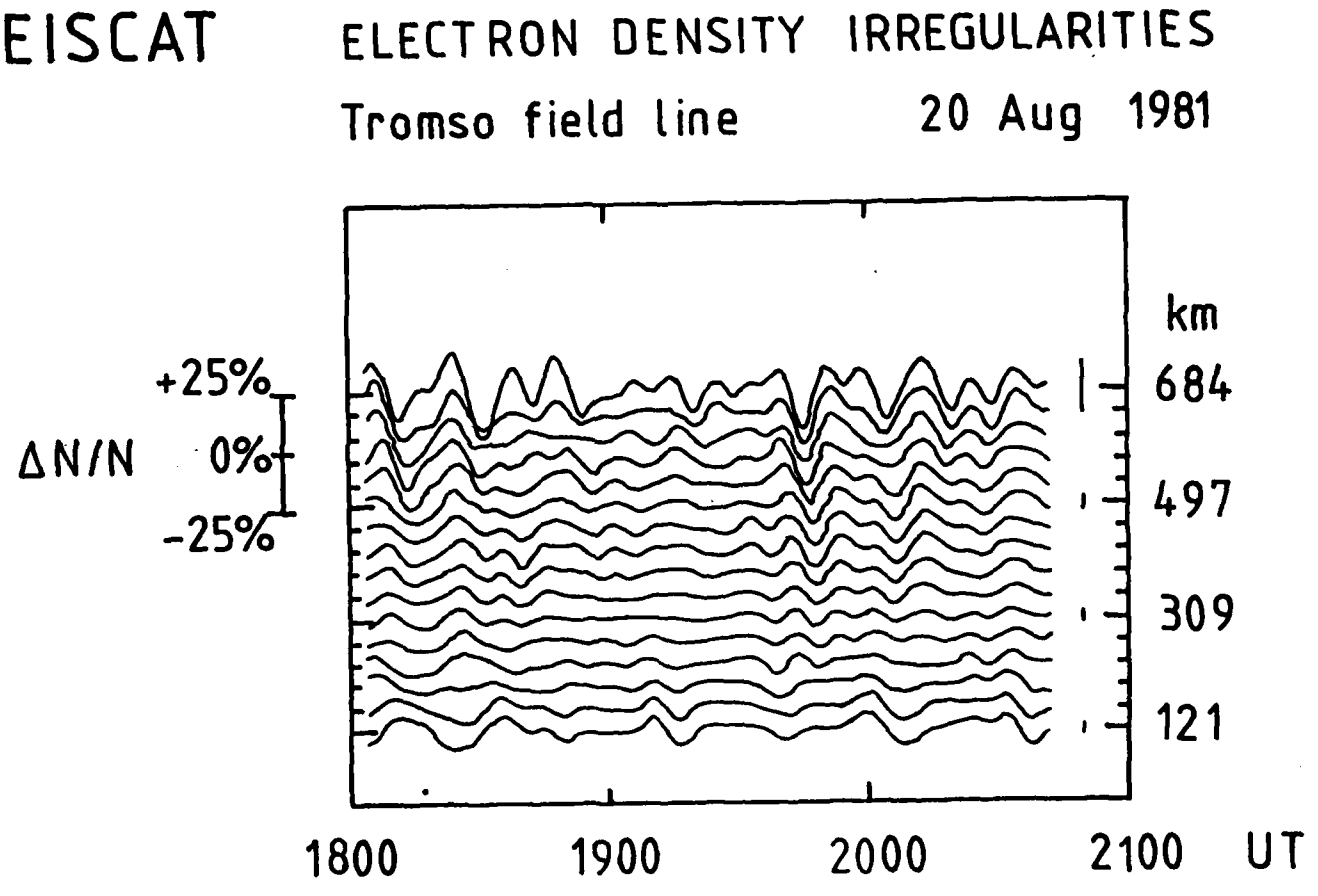
EISCAT
ELECTRON DENSITY IRREGULARITIES
Tromso field line
20 Aug 1981
+25%
ΔN/N
0%
-25%
km
684
497
309
121
1800
1900
2000
2100
UT

Figure 12

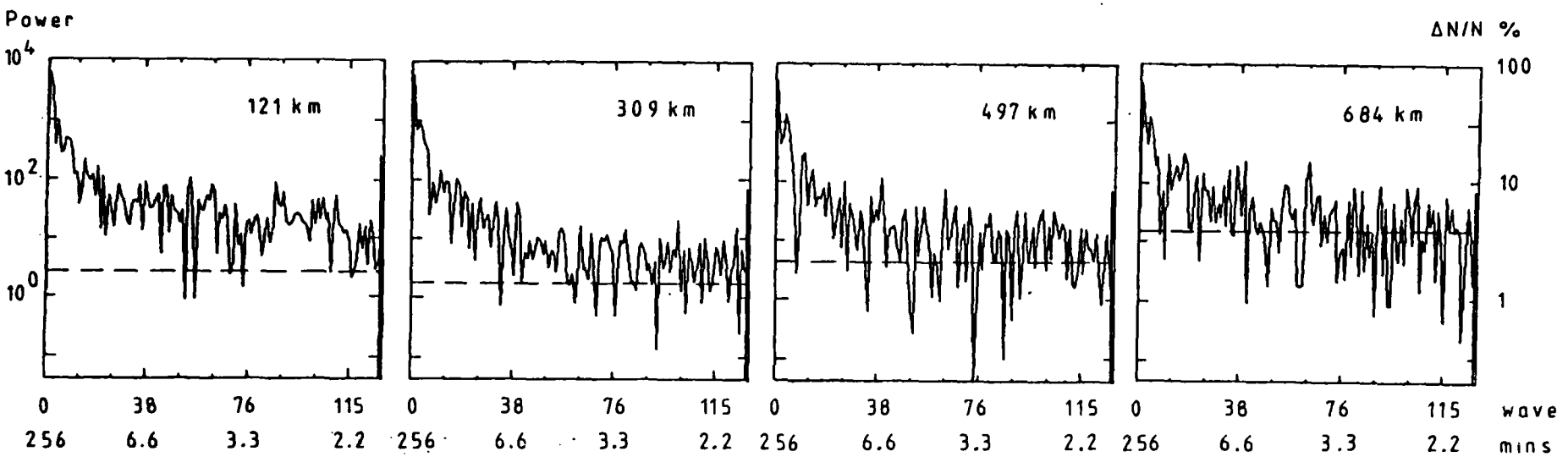
Power
10^4
10^2
10^0
121 km
309 km
497 km
684 km
ΔN/N %
100
10
1
0 38 76 115
256 6.6 3.3 2.2
wave no.
mins

Figure 13

Appendix 1:

Definition of first experiment

September 1981.

Related to EP 103.

Study of high-latitude F-region irregularities using EISCAT

Definition of first experiment

S.C. Kirkwood and J.K. Hargreaves

Environmental Sciences Dept.,

University of Lancaster.

Abstract

This note considers the sensitivity of the EISCAT UHF radar to small-scale F-region irregularities and specifies observations for the initial experiment.

Introduction

Irregularities in electron density in the high-latitude F-region have been much studied primarily because of their effects on radio communication (scintillation) but also because a knowledge of their form and distribution provides an insight into the dynamics of the polar ionosphere and magnetosphere.

Studies using ground based radio-wave observations and in situ satellite and rocket measurements have given a good indication of the geographical, time, seasonal and magnetic activity dependence of these irregularities and of their size distribution but the picture is not yet complete and no theory of their formation is generally accepted. Ground based observations detect only an effect integrated over the whole wave-path so that height distribution remains uncertain and the lateral distribution can only be modelled from its diffracting effects. Satellites and rockets take measurements only along a line so that time and space variations cannot be separated. We show here that EISCAT should provide the capability to measure electron density directly, with good enough time and space resolution to map the sizes, shapes and drift speeds of at least the larger scale irregularities ($> \sim 5$ km scale size), in favourable circumstances.

The most important information already available about the high latitude irregularity zone is summarized in Table 1. Dayside irregularities in the 65-75^{o} invariant latitude range should be the easiest to observe with EISCAT as they are generally the strongest, particularly in terms of absolute ΔN. It is hoped that the sub-auroral zone irregularities will also be resolvable as here there is particular interest in the drift pattern as an indication of whether irregularities have migrated from the auroral oval or have been formed in situ. High latitude F-region ion drift velocities are shown in Figure 1. These refer to plasma convection, which is not necessarily the same as irregularity drift. However, as only a few

observations of irregularity drift have been made, giving the same sort of velocities, Figure 1 will be used in planning measurements, as the drift may severely limit the possible resolution, and is outlined below.

Experimental Considerations

The amplitude of the irregularities seems generally to follow a power law relation to scale size, the largest scale sizes having the largest amplitudes. For example an (average) $(\Delta N/N)_{RMS}$ of 10% corresponds to $\frac{\Delta N}{N} \sim$ 20% for 100 km scale size, 10% for 50 km scale size and only 0.2% for 1 km scale size. Therefore the largest irregularities will be the easiest to resolve. If we aim to look at irregularities by a latitude or longitude scan then each measurement must be accurate enough that the uncertainty in the value of electron density ($\delta N/N$) is less than the relative irregularity amplitude ($\Delta N/N$) which we want to measure, i.e. the measurement integration time (T) increases as the scale size (wavelength) we want to detect (d) becomes smaller. In fact $T \simeq \alpha/d^2$, where α depends on signal/noise ratio (which depends on the state of the ionosphere and the EISCAT parameters) and the irregularity amplitudes (see Appendix).

If the irregularities do not drift and T is long enough, then the spatial resolution in a scan is the EISCAT beam-width or twice the distance between measurements, whichever is larger. However, if the irregularities drift while a measurement is being made then the resolution d_{res} is the largest of b, vT, and $2(\Delta x - v\Delta t)$, where Δx is the distance between measurements, b the beam width, v the drift velocity in the x direction, T integration time, Δt the time between the starts of successive measurements. It is assumed that the beam is stationary during each measurement.

Obviously, when there is drift (which will usually be the case) T has to be chosen as a compromise between spatial resolution (small T, Δt) and the detection of small-scale, weak irregularities (T large). Tables

showing the minimum scale size we can hope to resolve (both spatially and in amplitude) and corresponding integration times for likely ionospheric conditions are shown in Tables 2-3. Drift velocities oppositely directed to the beam scanning direction are assumed, as this represents the worst case and will always be so on one of a pair of forward and back scans. The EISCAT UHF beam-width is 0.6°. Ranges and signal/signal-plus-noise ratios are calculated by EISCAT planning program (P. Williams, T. van Eyken). In Table 3 pulse compression has been assumed - without this the effective beam-width (and scale length resolution) in the N-S direction would be $\sim$ 12 km (due to obliquity).

If we want to look directly at the sizes and drift speeds of individual features then they must be visible on at least two successive scans. Points to the right of the solid line in Tables 2a and 3a fall into this category. In order to look at irregularities in this way we will therefore have to select a time with high ionospheric electron density and low drift speed, or accept a scale-size resolution limit of $\sim$ 20 km.

If the irregularities are wave-like, i.e. if there are no sharp edges or large individual features, then their spectrum may not vary from place to place and we can study them statistically by looking at the scale size spectrum on several latitude and longitude scans. The minimum scale sizes which we can hope to resolve in this case are shown in Tables 2b and 3b. In the 1-D case the drift velocity can be derived simply from the shift in the spectrum for scans in opposite directions. In practice we will have to make assumptions about irregularity shape or use other independent information to derive 2-D drift velocities from the irregularity spectrum. In this case the scale size resolution is much less limited by high drift speeds even for more moderate ionospheric electron density so

that we might resolve down to 5 km even with drift speeds approaching 1 km/s.

Proposed Experiment

To select the most favourable time for an experiment (i.e. high electron density, low drift speeds, reasonable level of irregularity amplitudes) we note that scintillation studies have shown that irregularities occur most frequently if there is at least moderate magnetic activity, and, at least near 70°N, irregularities are likely to be stronger in winter. The drift speed will probably be lowest near noon or near midnight (Figure 1), but common programme ion drift measurements by EISCAT will be needed to confirm the pattern as previous measurements have been at North American longitudes, and longitude/U.T. dependence is expected. Electron density in the high latitude zone is largely unknown and here EISCAT's own measurements will be most important.

If electron densities $\sim 4 \times 10^{12}$ are common then we can look directly at individual irregularities. A suggested sequence of measurements for the auroral zone is shown in Table 4 - this involves scans northward and back, eastward and back, starting from a point at 66.5°N (invariant) on the Tromsø magnetic meridian near midnight and near noon. The scans are about 100 km long at 325 km altitude, measurements being made every 2 km. An experiment would consist of a scan north and back, and east and back (taking nearly 10 minutes), followed by 5-minutes observation with the beam fixed at the starting point. The whole sequence would be repeated 4 times, giving an experiment duration of 1 hour. Note that 0.3 secs have been allowed in Table 4 to move the antennas from one position to the next. An increase in this time to about 2 secs could be tolerated provided the ionospheric drift velocity is less than 0.2 m/s, with less than 1 km

increase in the scale-size resolution. In later experiments similar sequences of measurements would be made starting near 63 ^{o}N and 70^{o}N on the Tromsø meridian.

If electron densities are generally too low for the direct model, then shorter integration times, at closer spacing, would be more appropriate with statistical analysis of the irregularity spectrum. A suggested sequence is given in Table 5. Including 5-minute periods with the beam fixed, this experiment would take 75 minutes. Again an increase in the time taken to move between positions to about 2 secs could be tolerated, even at moderate drift speeds (up to 0.4 km/s) with the scale size resolution increasing to $\sim$ 5 km.

If possible, all scans should be accompanied by tristatic plasma drift measurements.

Appendix

Calculation of minimum resolvable scale size

a) The uncertainty in a measurement of electron density made by an incoherent scatter radar is given by

$$\frac{\delta N}{N} = \frac{\delta Ps}{Ps} = \frac{Ps + Pn}{Ps\sqrt{nB\tau}} \qquad (^{5}\text{Evans, 1969})$$

where Ps and Pn are the signal and noise power respectively, and n is the number of times the measurement is repeated (i.e. the number of pulses), τ is the pulse length and B the receiver bandwidth. Ps depends on the peak beam power ($\hat{P}$), the antenna effective area (A), the distance to the scattering point (h), the pulse length (τ), the electron cross-section (σ), the cable loss factor (l), electron and ion temperatures (Te, Ti), the electron density (N)

$$P_s = \frac{\hat{P}\, A\, N\, \sigma\, c\, \tau\, l^2}{50\, h^2\, (1 + Te/Ti)} \qquad (c=\text{speed of light})$$

The noise power depends on the receiver bandwidth (B) and 'noise' temperature Tn

$$P_n = kT_n B \qquad (k=\text{Boltzman's constant})$$

where B is the pulse bandwidth (τ^{-1}) or ion line bandwidth ($B_i \simeq 4/\lambda\sqrt{8RT_i/M_i}$), whichever is largest (λ is radio wavelength, M_i ion mass, R the gas constant).

The best (lowest) values of $\delta N/N$ we can obtain in a given time will be achieved by using the maximum pulse repetition frequency and the longest pulse length which is consistant with the available peak/mean power ratio. This ratio is about 10 for EISCAT, and the p.r.f. is 1000 Hz, giving a maximum pulse length of $\sim$ 100 μS. Using these values we can write

$$\frac{\delta N}{N} = \beta/\sqrt{T} \qquad (1)$$

where β is a constant for any given measurement, at particular coordinates in constant ionospheric conditions, T is the integration time ($\simeq$ n/p.r.f.)

The EISCAT planning program (T. van Eyken, P. Williams) can be used to calculate β for any given coordinates and likely ionospheric conditions. This program gives the integration time necessary to achieve a $\delta N/N$ of 5%, say $T_{5\%}$. Equation (1) then gives

$$\beta = \frac{5}{100}\sqrt{T_{(5\%)}} \qquad (2)$$

b) The amplitude of electron density irregularities in the high latitude F-region seems to be related to scale size by a power law

$$A(d) \approx (\Delta N/N)_{RMS} \times d/50$$

where A(d) is the 'amplitude' of the irregularities with scale size d, $(\Delta N/N)_{RMS}$ is the RMS irregularity amplitude, for scale sizes $\sim$ 1 - 100 km. The integration time needed to make a measurement of electron density accurate enough to detect an irregularity of this amplitude is, from (1)

$$T = \beta^2/\left(\frac{\delta N}{N}\right)^2 = \beta^2/A(d)^2$$

$$T = 50^2\beta^2/(\Delta N/N)^2_{RMS}d^2 \qquad (3)$$

Irregularities may occur as wave-like disturbances so that even if their amplitude (A(d)) were less than the uncertainty in the electron density measurements ($\delta N/N$) they might still be resolvable using, for example, filtering to remove the ($\delta N/N$) 'noise'. In this case several 'cycles' of irregularity are effectively stacked and the 'noise' reduced by a factor $\sqrt{m}$, where m is the number of cycles stacked. Equation (1) can be rewritten

$$\left(\frac{\delta N}{N}\right)_{stacked} = m^{-\frac{1}{2}}\,\beta/\sqrt{T} \qquad (4)$$

leading to a slightly different version of (3)

$$T_{stacked} = 50^2\,\beta^2/(\Delta N/N)^2_{RMS}Dd \qquad (5)$$

where D/d has been substituted for m, D being the distance over which the train of irregularity 'waves' has been measured.

c) Spatial resolution in a latitude or longitude scan.

If the pattern of irregularities is stationary the smallest scale size resolvable in a scan is twice the distance between the points at which measurements are made. If the pattern drifts then the effective distance between measurements is increased or decreased according to how the pattern drifts between measurements

$$\Delta X_{effective} = \Delta X - vt$$

where ΔX is the actual distance moved, v the drift velocity in the $+\Delta X$ direction, t the time between successive measurements. t can be written as

$$t = T + \Delta X/S$$

where T is the time taken making the measurement, the integration time, and $\Delta X/S$ the time taken to move to the next position, with S the antenna slewing 'velocity' at the point where measurements are being made.

The spatial resolution as determed by the measurement spacing is then given by:

$$d_{min_X} = 2\,\Delta X_{effective} = 2\Delta X - 2v(T + \Delta X/S) \qquad (6)$$

The spatial resolution may be further limited by the spatial filtering effects due to the antenna beam width, or averaging over the distance the pattern drifts during a measurement. These give:

$d_{min_b} = b$ where b is the beam width (3.4 km at range 325 km) (7)

$d_{min_T} = vT$ where v is the drift velocity, T the integration time (8)

The shortest resolvable scale size in practice will be the largest of these three.

d) Minimum resolvable irregularity scale size.

The minimum resolvable irregularity scale size is found by simultaneous solution of Equations (3) and (6), for the case of individual irregularities and Equations (5) and (6) for wave-like irregularities (unless the

filtering restrictions (7) and (8) imply a longer scale size). This gives:

for individual irregularities to be resolvable:

$$d_{min}^2 \, (d_{min} - 2\Delta X + 2v \, \Delta X/S) = \frac{-2V \, 5O^2 \beta^2}{(\Delta N/N)^2_{RMS}}$$

and for wave-like irregularities:

$$d_{min} \, (d_{min} - 2\Delta X + 2V \, \Delta X/S) = \frac{-2V \, 5O^2 \beta^2}{(\Delta N/N)^2_{RMS} D}$$

Table 1 High latitude irregularity characteristics. Note that upper limit to altitude range is upper limit of observations, not necessarily limit of irregularities. Except where marked, information is from Clark and Raitt, 1975 and 1976 [6,7].

Zone	Location	Average Intensity $(\Delta N/N)_{RMS}$	Occurrence	Possible Production Mechanism
polar zone	>72°-84°, midnight >65°-82°, noon [3]varies with magnetic activity	moderate - strong (6-10%)	all times, all altitudes (400[2]-3500[1] km) all times, all altitudes (350[2]-3500[1] km)	poleward motion of irregularities generated in auroral zone 1) particle precipitation 2) electrostatic turbulence 3) [4]plasma instabilities
auroral zone	64°-74°N, midnight 72°-74°N, noon for Kp ~ 3	strong (8-10%)	Increasing intensity and equatorward movement of boundary with increasing Kp	
sub auroral zone	between 50°-60° and 64°N, midnight	moderate (4-6%)	only at night, all altitudes (300[2]-3500[1] km) Equatorward movement of boundary with increasing Kp.	1) [4]equatorial motion from creation in auroral zone 2) magnetospheric heat conduction 3) heat transfer from ring current 4) heating effect of conjugate photo electrons in winter

[1]Phelps, A.D.R., Sagalyn, R.C., 1976
[2]Frihagen, J., 1970.
[3]Sandford, B.P. 1970
[4]Fejer, B.G., Kelley, M.C., 1980.

Table 2a. Minimum resolvable irregularity scale sizes near 66.5°N (invariant)

	Δx = 0 km Δt = 0.0s		Δx = 1 km Δt = 0.1s		Δx = 2 km Δt = 0.3s		Δx = 4 km Δt = 0.5s		Δx = 8 km Δt = 1.1s	
	d_{min}	T	d_{min}	T	d_{min}	T	d_{min}	T	d_{min}	T
v = 0.0 km/s	-	-	3.4	54	4.0	39	8.0	9.8	16	2.4
1.1 km/s	5.0	25	6.0	17	6.8	14	9.5	6.9	17	2.2
0.2 km/s	6.3	16	7.2	12	8.3	9.1	11	5.2	17	2.2
0.4 km/s	7.9	10	8.7	8.3	9.8	6.5	12	4.3	19	1.7
0.8 km/s	10	6.3	11	5.2	12	4.3	15	2.8	22	1.3

Electron density at 325 km: 3×10^{11} m^{-3}, $T_{5\%}$ = 1s

	Δx = 0 km Δt = 0.0s		Δx = 1 km Δt = 0.1s		Δx = 2 km Δt = 0.3s		Δx = 4 km Δt = 0.5s		Δx = 8 km Δt = 1.1s	
	d_{min}	T	d_{min}	T	d_{min}	T	d_{min}	T	d_{min}	T
v = 0.0 km/s	-	-	3.4	5.4	4.0	3.9	8.0	1.0	16	0.2
0.1 km/s	3.4	5.4	3.6	4.8	5.1	2.4	8.3	0.9	16	0.2
0.2 km/s	3.4	5.4	3.9	4.1	5.4	2.1	8.5	0.9	16	0.2
0.4 km/s	3.7	4.6	4.5	3.1	5.8	1.9	9.1	0.8	17	0.2
0.8 km/s	4.6	3.0	5.6	2.1	6.8	1.4	10	0.6	18	0.2

Electron density at 325 km: 4×10^{12} m^{-3}, $T_{5\%}$ = 0.1s

Table 2b. Minimum resolvable irregularity scale sizes near 66.5°N (invariant)

	Δx = 0 km Δt = 0.0s		Δx = 1 km Δt = 0.1s		Δx = 2 km Δt = 0.3s		Δx = 4 km Δt = 0.5s		Δx = 8 km Δt = 1.1s	
	d_{min}	T	d_{min}	T	d_{min}	T	d_{min}	T	d_{min}	T
v = 0.0 km/s	-	-	3.4	1.8	4.0	1.6	8.0	0.8	16	0.4
0.1 km/s	3.4	1.8	3.4	1.8	4.4	1.5	8.2	0.8	16	0.4
0.2 km/s	3.4	1.8	3.4	1.8	4.6	1.4	8.6	0.8	17	0.3
0.4 km/s	3.4	1.8	3.5	1.8	5.2	1.2	9.0	0.7	17	0.3
0.8 km/s	3.4	1.8	4.4	1.5	6.0	1.0	9.8	0.7	18	0.3

Electron density at 325 km: 3×10^{11} m^{-3}, $T_{5\%}$ = 1s

	Δx = 0 km Δt = 0.0s		Δx = 1 km Δt = 0.1s		Δx = 2 km Δt = 0.3s		Δx = 4 km Δt = 0.5s		Δx = 8 km Δt = 1.1s	
	d_{min}	T	d_{min}	T	d_{min}	T	d_{min}	T	d_{min}	T
v = 0.0 km/s	-	-	3.4	.18	4.0	.16	8.0	.08	16	.04
0.1 km/s	3.4	.18	3.4	.18	4.1	.15	8.1	.08	16	.04
0.2 km/s	3.4	.18	3.4	.18	4.2	.15	8.2	.08	16	.04
0.4 km/s	3.4	.18	3.4	.18	4.4	.14	8.5	.07	17	.04
0.8 km/s	3.4	.18	3.4	.18	4.6	.13	8.9	.07	18	.03

Electron density at 325 km: 4×10^{12} m^{-3}, $T_{5\%}$ = 0.1s

Tables 2a and 2b

Minimum resolvable irregularity scale size d_{min} (km) assuming a level of irregularities $(\Delta N/N)_{RMS}$ = 10% for (a) isolated irregularities, where the minimum detectable 'amplitude' is determined by the uncertainty in measuring the electron density and (b) wave-like irregularities, which can be detected with an amplitude less than the uncertainty in electron density using spectral analysis and/or filtering. In calculating the values in these tables we have used a beam scan speed of 80°/min, a length of scan of 100 km, starting directly overhead at Tromsø. Δx is distance between beam positions at 325 km altitude, Δt is the time taken to move the beam through Δx, T is integration time (secs), v is irregularity drift velocity, assumed anti-parallel to the beam scanning direction. Points to the right of the solid line are those where features could be identified on two successive scans.

Table 3a Minimum resolvable irregularity scale sizes near 70°N or 63°N (invariant)

	Δx = 0 km Δt = 0.0s		Δx = 1 km Δt = 0.1s		Δx = 2 km Δt = 0.2s		Δx = 4 km Δt = 0.3s		Δx = 8 km Δt = 0.7s	
	d_{min}	T	d_{min}	T	d_{min}	T	d_{min}	T	d_{min}	T
v = 0.0 km/s	-	-	5.3	33	5.3	33	8.0	15	16	4
0.1 km/s	5.7	29	6.6	22	7.4	17	10	9	17	3
0.2 km/s	7.2	18	8.0	15	9	12	11	8	18	3
0.4 km/s	9.1	11	10	9	11	8	13	6	19	3
0.8 km/s	11	8	12	7	13	6	15	4	22	2

Electron density at 325 km: 3×10^{11} m^{-3}, $T_{5\%}$ = 1.5s

	Δx = 0 km Δt = 0.0s		Δx = 1 km Δt = 0.1s		Δx = 2 km Δt = 0.2s		Δx = 4 km Δt = 0.3s		Δx = 8 km Δt = 0.7s	
	d_{min}	T	d_{min}	T	d_{min}	T	d_{min}	T	d_{min}	T
v = 0.0 km/s	-	-	5.3	3.1	5.3	3.1	8.0	1.4	16	0.3
0.1 km/s	5.3	3.1	5.3	3.1	5.3	3.1	8.3	1.3	16	0.3
0.2 km/s	5.3	3.1	5.3	3.1	5.5	2.9	8.6	1.2	16	0.3
0.4 km/s	5.3	3.1	5.3	3.1	6.2	2.3	9.1	1.1	17	0.3
0.8 km/s	5.3	3.1	6.4	2.1	7.2	1.7	10	0.9	18	0.3

Electron density at 325 km: 4×10^{12} m^{-3}, $T_{5\%}$ = .15s

Table 3b Minimum resolvable irregularity scale sizes near 70°N or 63°N (invariant)

	Δx = 0 km Δt = 0.0s		Δx = 1 km Δt = 0.1s		Δx = 2 km Δt = 0.2s		Δx = 4 km Δt = 0.3s		Δx = 8 km Δt = 0.7s	
	d_{min}	T	d_{min}	T	d_{min}	T	d_{min}	T	d_{min}	T
v = 0.0 km/s	-	-	5.3	1.8	5.3	1.8	8.0	1.2	16	0.6
0.1 km/s	5.3	1.8	5.3	1.8	5.3	1.8	8.3	1.1	16	0.6
0.2 km/s	5.3	1.8	5.3	1.8	5.3	1.8	8.6	1.1	16	0.6
0.4 km/s	5.3	1.8	5.3	1.8	5.5	1.7	9.1	1.0	17	0.6
0.8 km/s	5.3	1.8	5.3	1.8	6.6	1.4	10	0.9	18	0.5

Electron density at 325 km: 3×10^{11} m^{-3}, $T_{5\%}$ = 1.5s

	Δx = 0 km Δt = 0.0s		Δx = 1 km Δt = 0.1s		Δx = 2 km Δt = 0.2s		Δx = 4 km Δt = 0.3s		Δx = 8 km Δt = 0.7s	
	d_{min}	T	d_{min}	T	d_{min}	T	d_{min}	T	d_{min}	T
v = 0.0 km/s	-	-	5.3	.18	5.3	.18	8.0	.12	16	.06
0.1 km/s	5.3	.18	5.3	.18	5.3	.18	8.1	.12	16	.06
0.2 km/s	5.3	.18	5.3	.18	5.3	.18	8.2	.11	16	.06
0.4 km/s	5.3	.18	5.3	.18	5.3	.18	8.3	.11	17	.06
0.8 km/s	5.3	.18	5.3	.18	5.3	.18	8.7	.11	17	.06

Electron density at 325 km: 4×10^{12} m^{-3}, $T_{5\%}$ = .15s

Tables 3a and 3b

Minimum resolvable irregularity scale size d_{min} (km) assuming a level of irregularities $(\Delta N/N)_{RMS}$ = 10% for (a) isolated irregularities, where the minimum detectable 'amplitude' is determined by the uncertainty in measuring the electron density and (b) wave-like irregularities, which can be detected with an amplitude less than the uncertainty in electron density using spectral analysis and/or filtering. In calculating the values in these tables we have used a beam scan speed of 80°/min, a length of scan of 100 km, starting 3.5° north or south of Tromsø. Δx is distance between beam positions at 325 km altitude, Δt is the time taken to move the beam through Δx, T is integration time (secs), v is irregularity drift velocity, assumed anti-parallel to the beam scanning direction. Points to the right of the solid line are those where features could be identified on two successive scans.

Table 4 Scanning sequence to study irregularities in high ambient ionospheric electron density (4×10^{12} m^{-3})

Starting at altitude 325 km, directly over Tromsø.

Pointing position given in km N and km E of starting position at 325 km altitude. Electron density measurements made at 300 km altitude, and 25 km intervals to 600 km altitude.

Pointing Sequence			Measurement details	
n	km N	km E	measurement start time	integration time
1	0	0	0s	2.5s
2	2	0	2.8 s	"
3	4	0	5.6 s	"
n	2(n-1)	0	2.8(n-1)s	"
50	98	0	140 s	"
51	100	0	142.8 s	"
52	98	0	145.6 s	"
n	2(102-n)	0	2.8(n-1)s	"
100	4	0	280 s	"
101	2	0	262.8 s	"
102	0	0	285.6 s	"
103	0	2	288.4 s	"
104	0	4	291.2 s	"
n	0	2(n-102)	2.8(n-1)s	"
151	0	98	422.8 s	"
152	0	100	425.6 s	"
153	0	98	428.4 s	"
n	0	2(203-n)	2.8(n-1)s	"
201	0	4	562.8 s	"
202	0	2	565.6 s	"
203	0	0	568.4 s	2.5s

Table 5 Scanning sequence to study irregularities in moderately high ambient ionospheric electron density. (3×10^{11} m^{-3})

Starting point at altitude 325 km, directly over Tromsø.
Pointing position given in km N and km E of starting point at 325 km altitude. Electron density measurements made at 300 km altitude and 25 km intervals to 600 km altitude.

Pointing Sequence			Measurement details	
n	km N	km E	measurement start time	integration time
1	0	0	0s	1.8s
2	1	0	2s	"
3	2	0	4s	"
n	1(n-1)	0	2(n-1) s	"
100	99	0	198 s	"
101	100	0	200 s	"
102	99	0	204 s	"
n	1(202-n)	0	2(n-1) s	"
200	2	0	398 s	"
201	1	0	400 s	"
202	0	0	402 s	"
203	0	1	404 s	"
204	0	2	406 s	"
n	0	1(n-202)	2(n-1) s	"
301	0	99	600 s	"
302	0	100	602 s	"
303	0	99	604 s	"
n	0	1(403-n)	2(n-1) s	"
401	0	2	800 s	"
402	0	1	802 s	"
403	0	0	804 s	"

References

1. Phelps, A.D.R., Sagalyn, R.C. Plasma density irregularities in the high latitude topside ionosphere. J. Geophys. Res. 81, 515-523, 1976.

2. Frihagen, J. Irregularities in the electron density of the polar ionosphere. In: The polar ionosphere and magnetospheric processes, G. Skovli, ed.: pp 271-284. New York: Gordon and Breach 1970.

3. Sandford, B.P. Optical emission over the polar cap. In: The polar ionosphere and magnetospheric processes, G. Skovli, ed.: pp 299-321 New York: Gordon and Breach 1970.

4. Fejer, B.G., Kelley, M.C. Ionospheric irregularities. Rev. Geophys. Space Phys. 18, 401-454, 1980.

5. Evans, J.V. Theory and practice of ionospheric study by Thomson scatter radar. Proc. IEEE 57, 496-517, 1969.

6. Clark, D.H. Raitt, W.J. Characteristics of the high latitude ionospheric irregularity boundary as monitored by the total ion current probe on Esro-4. Planet. Space Sci. 23, 1643-1647, 1975.

7. Clark, D.H., Raitt, W.J. The Global morphology of irregularities in the topside ionosphere as measured by the total ion current probe on Esro 4. Planet. Space Sci. 24, 873-881, 1976.

8. Evans, J.V., Holt, J.M., Oliver, W.L., Wand, R.H. Millstone Hill incoherent scatter observations of auroral convection over $60^{\circ} < \Lambda < 75^{\circ}$, 2.Initial results. J. Geophys. Res. 85, 41-54, 1980.

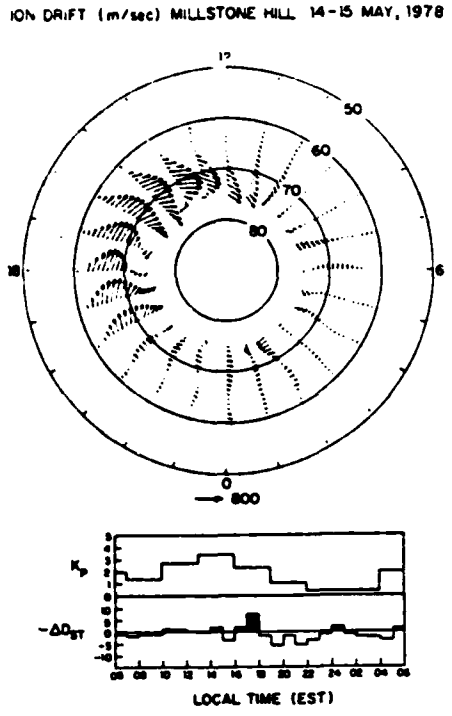

Fig. 6. Drift pattern of *F* region plasma observed on May 14–15, 1978, over $60° \leq \Lambda \leq 75°$ from Millstone Hill versus geographic local time. Also given is the *Kp* index and the change in the hourly values of *Dst*.

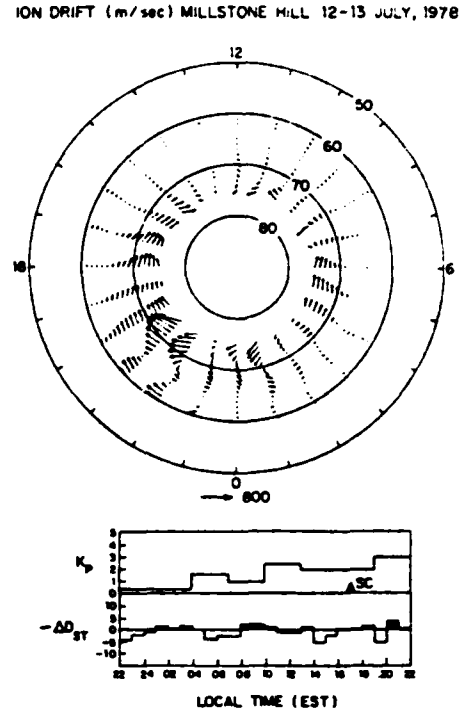

Fig. 8. Drift pattern of *F* region plasma observed on July 12–13, 1978, over $60° \leq \Lambda \leq 75°$ from Millstone Hill versus geographic local time. Also given is the *Kp* index and the change in the hourly values of *Dst*.

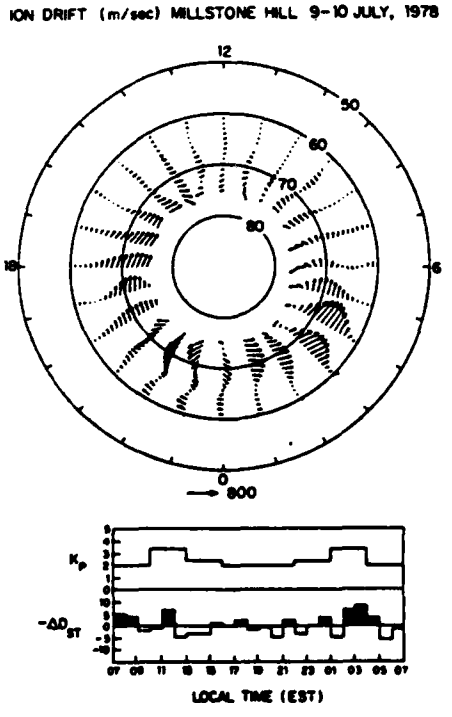

Fig. 7. Drift pattern of *F* region plasma observed on July 9–10, 1978, over $60° \leq \Lambda \leq 75°$ from Millstone Hill versus geographic local time. Also given is the *Kp* index and the change in the hourly values of *Dst*.

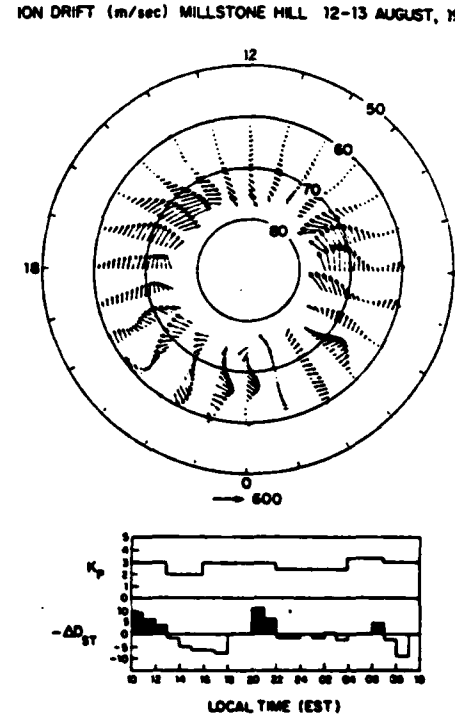

Fig. 9. Drift pattern of *F* region plasma observed on August 12–13, 1978, over $60° \leq \Lambda \leq 75°$ from Millstone Hill versus geographic local time. Also given is the *Kp* index and the change in the hourly values of *Dst*.

Figure 1 from Evans et al. 1980[8]

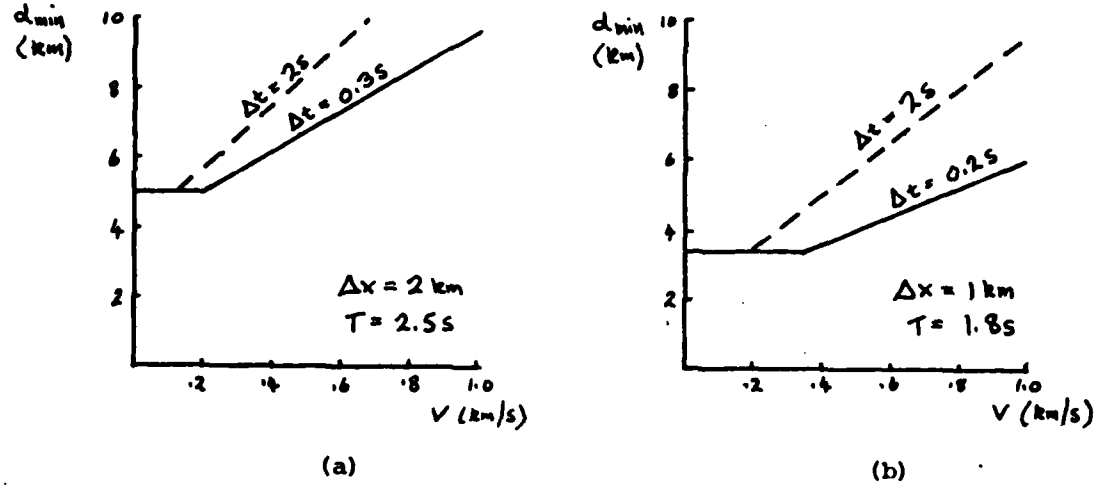

Figure 2. Minimum resolvable scale sizes as a function of drift velocity for the scanning sequences in (a) Table 4 and (b) Table 5. The lower values of Δt are those used in Tables 4 and 5. The dashed line (higher Δt) shows the reduction in resolution if the time taken to move the beam from one position to the next (Δt) is much longer than the minimum (2s).